Light Harvesting in Photosystem I: Modeling Based on the 2.5-Å Structure of Photosystem I from *Synechococcus elongatus*

Martin Byrdin,*† Patrick Jordan,‡ Norbert Krauss,‡ Petra Fromme,†§ Dietmar Stehlik,* and Eberhard Schlodder†

*Institut für Experimentalphysik, Freie Universität Berlin, D-14195 Berlin, Germany; †Max-Volmer-Laboratorium für Biophysikalische Chemie, Technische Universität Berlin, D-10623 Berlin, Germany; ‡Institut für Chemie und Kristallographie, Freie Universität Berlin, D-14195 Berlin, Germany; and §Department of Chemistry and Biochemistry, Arizona State University, Tempe, AZ 85287 USA

ABSTRACT The structure of photosystem I from the thermophilic cyanobacterium *Synechococcus elongatus* has been recently resolved by x-ray crystallography to 2.5-Å resolution. Besides the reaction center, photosystem I consists also of a core antenna containing 90 chlorophyll and 22 carotenoid molecules. It is their function to harvest solar energy and to transfer this energy to the reaction center (RC) where the excitation energy is converted into a charge separated state. Methods of steady-state optical spectroscopy such as absorption, linear, and circular dichroism have been applied to obtain information on the spectral properties of the complex, whereas transient absorption and fluorescence studies reported in the literature provide information on the dynamics of the excitation energy transfer. On the basis of the structure, the spectral properties and the energy transfer kinetics are simultaneously modeled by application of excitonic coupling theory to reveal relationships between structure and function. A spectral assignment of the 96 chlorophylls is suggested that allows us to reproduce both optical spectra and transfer and emission spectra and lifetimes of the photosystem I complex from *S. elongatus*. The model calculation allowed to study the influence of the following parameters on the excited state dynamics: the orientation factor, the heterogeneous site energies, the modifications arising from excitonic coupling (redistribution of oscillator strength, energetic splitting, reorientation of transition dipoles), and presence or absence of the linker cluster chlorophylls between antenna and reaction center. For the Förster radius and the intrinsic primary charge separation rate, the following values have been obtained: $R_0 = 7.8$ nm and $k_{CS} = 0.9\ ps^{-1}$. Variations of these parameters indicate that the excited state dynamics is neither pure trap limited, nor pure transfer (to-the-trap) limited but seems to be rather balanced.

INTRODUCTION

In photosynthesis, solar energy is captured by light-harvesting antennae and transferred to the reaction center (RC) where it is used for transmembrane charge separation.

Light harvesting proceeds with a quantum efficiency of almost one. Recent emergence of the structures of a growing number of pigment-protein complexes (Deisenhofer et al., 1985; Kühlbrandt et al., 1994; McDermott et al., 1995; Koepke et al., 1996; Zouni et al., 2001; Jordan et al., 2001) stimulated numerous spectroscopic investigations as well as theoretical studies (van Grondelle et al., 1994; Arnett et al., 1999; Sundström et al., 1999; Schulten, 1999; van Amerongen et al., 2000; and references therein) analyzing relationships between structural features and functional properties.

Submitted December 27, 2001, and accepted for publication March 26, 2002.

Address reprint requests to Eberhard Schlodder, Max-Volmer-Laboratorium für Biophysikalische Chemie, Technische Universität Berlin, Strasse des 17. Juni 135, D-10623 Berlin, Germany. Tel.: 49-30-31422688; Fax: 49-30-31421122; E-mail: e.schl@struktur.chem.tu-berlin.de or to Dietmar Stehlik, Institut für Experimentalphysik, Freie Universität Berlin, Arnimallee 14, D-14195 Berlin, Germany. Tel.: 49-30-83855069; Fax: 49-30-83856081; E-mail: stehlik@physik.fu-berlin.de.

Norbert Krauss's present address is Institut für Biochemie, Universitätsklinikum Charité, Medizinische Fakultät der Humboldt-Universität zu Berlin, Monbijoustr. 2, D-10117 Berlin, Germany.

0006-3495/02/07/433/25 $2.00

With photosystem I (PS I) from *Synechococcus elongatus*, for the first time a high resolution x-ray structure becomes available for a photosynthetic pigment-protein complex that binds both light harvesting antenna pigments and the reaction center cofactors inseparably on the same protein subunits. It is a unique property of the PS I complex that it carries out all the primary photosynthetic processes within one and the same membrane protein complex. Thus, it offers the possibility to study the interplay of light absorption, excited state energy transfer, and trapping by electron transfer within one functional unit.

PS I is a membrane-bound pigment-protein complex that mediates the light-driven electron transfer from reduced plastocyanine or cytochrome c_6 to ferredoxin or flavodoxin (for review, see Golbeck, 1994; Brettel, 1997). The PS I complex of cyanobacteria is composed of 12 subunits. The two largest subunits (PsaA and PsaB) bind most of the antenna pigments and the following redox cofactors involved in the electron-transfer process: the primary electron donor P700 (a heterodimer of chlorophyll $a(P_B)$ and $a'(P_A)$, the primary acceptor A_0 (a Chl *a* monomer), the secondary acceptor A_1 (a phylloquinone), and F_X (a [4Fe-4S] iron sulfur cluster). The terminal electron acceptors F_A and F_B (two [4Fe-4S] iron sulfur clusters) are both coordinated by subunit PsaC, one of the three extrinsic subunits located on the stromal side.

The recently published x-ray structure of PS I from *S. elongatus* at 2.5-Å resolution (Jordan et al., 2001) identifies

TABLE 1 Number of Chls and mean nearest neighbor distances of pigment-protein-complexes

Pigment-protein-complex	Reference	Pdb-file	Number of (Bacterio-) chlorins	Mean nearest neighbor distance Å
LH2 B850 ring	McDermott et al. 1995	1KZU	18	9.2 ± 0.0
LHC II	Kühlbrandt et al. 1994		12	9.5 ± 1.3
bRC	Deisenhofer et al. 1985	1PRC	6	9.5 ± 1.7
PS I	Jordan et al. 2001	1JB0	96	9.9 ± 2.2
PS II	Zouni et al. 2001	1FE1	34	10.9 ± 2.9
FMO	Fenna and Matthews 1975	4BCL	7	11.8 ± 0.6

The errors indicated represent the statistical spread of 1 SD.

twelve protein subunits, 96 Chls, 22 carotenoids (Car), two phylloquinones, three iron-sulfur clusters, four lipids, ~200 water molecules, and a metal ion (presumably Ca^{2+}). Knowledge of the detailed arrangement of the Chls makes it possible to calculate the mutual orientation of the Q_Y optical transition moments and allows to abandon the use of just averaged orientation values for theoretically predicted excitation energy transfer rates between individual pigments. This is a big step forward towards a more realistic description of the excitation energy transfer in PS I. Although, there is still left some uncertainty as long as the Förster overlap integrals (FOI) are not exactly known due to lack of knowledge on the exact spectral line positions and shapes of all Chls embedded in the protein environment and on the local dielectric constant of the protein environment.

Most of the Chls are rather densely packed within two layers at the membrane surfaces. The antenna system has been divided spatially into a central and two peripheral domains (Jordan et al., 2001). The central domain surrounds the five C-terminal α-helices of PsaA and PsaB, which coordinate the cofactors involved in electron transfer. It also contains 10 Chls that are located between the stromal and lumenal layers, thereby facilitating excitation energy transfer between them.

A comparison of the mean distances between nearest neighbor Chls shows that the PS I complex is well within the values for other structurally known pigment-protein complexes (Table 1). In all cases the mean nearest neighbor distance is only slightly above the ~9-Å diameter of the chlorin ring of the Chls.

Up to now, various attempts have been made to explain spectral properties of pigment-protein complexes in terms of excitonically interacting chromophores not only for the systems with smaller center-to-center distances (rows 1–3 in Table 1; Sundström et al., 1999; Gradinaru et al., 1998; Knapp et al., 1985), but also for the Femma–Mathews–Olson (FMO)-complex (last row in Table 1) with considerable larger center-to-center distances (Pearlstein, 1992; van Amerongen et al., 2000; Owen and Hoff, 2001).

From the mean nearest neighbor distance of 9.9 Å in the PS I complex, an average interaction energy between neighboring Chls of ~70 cm^{-1} is calculated, which corresponds to ~6 nm splitting between the upper and lower excitonic bands. Due to the magnitude of the exciton coupling between each pigment and its nearest neighbor the spectral properties may be described by exciton states partially delocalized over the pigments. Therefore, it is essential to take into account excitonic interaction for the characterization of the electronic excited state of antenna pigments. Various spectroscopic observations have been interpreted as indication for excitonic interactions between Chls in PS I from *Synechocystis* (Gobets et al., 1994; Savikhin et al., 1999, 2000; Melkozernov et al., 2000; Rätsep et al., 2000) and *Spirulina platensis* (Engelmann et al., 2001).

In addition, the short center-to-center distances between the Chls suggest very fast energy transfer and charge separation kinetics. Indeed, a single step rate constant of energy transfer from Chl to Chl has been estimated to be ~200 fs^{-1}, (Du et al., 1993). The fluorescence lifetime of PS I from *S. elongatus* has been found to be between 33 and 38 ps in good agreement between various groups (Holzwarth et al., 1993; Dorra et al., 1998; Byrdin et al., 2000; Gobets et al., 2001; Kennis et al., 2001). It has been attributed to the trapping of excitation energy via charge separation. The spectrum associated with the trapping is positive at all wavelengths and was found to be independent of the excitation wavelength (Hastings et al., 1995; Melkozernov et al., 2000). As the Chls in PS I absorb at different wavelengths, excited state energy redistribution processes directed towards thermal equilibration take place, the slowest of which have been detected with transfer lifetimes in the 2- to 15-ps range (Holzwarth et al., 1993; Dorra et al., 1998; Byrdin et al., 2000; Gobets et al., 2001; Kennis et al., 2001). The spectra associated with energy redistribution processes exhibit positive and negative amplitudes related to energy transfer between antenna Chls absorbing at different wavelengths. The shape of these spectra are strongly excitation wavelength dependent (Hastings et al., 1995; Melkozernov et al., 2000).

Regarding the spectral heterogeneity, the most intriguing feature of the PS I complex is that it contains so called "red" chlorophylls that absorb at wavelengths above 700 nm, i.e., at energies below that of the primary donor P700. Time-resolved fluorescence measurements with samples of vary-

ing red Chl content (Gobets et al., 2001) as well as numerous previous studies (e.g., Trissl, 1993; Trinkunas and Holzwarth, 1996; Pålsson et al., 1998; Byrdin et al., 2000; Gobets et al., 2001) indicate a crucial role of these red Chls in the kinetics of energy transfer and trapping. At present, it is not clear which Chls are responsible for the long wavelength absorption. Unfortunately, even a high-resolution structure does not allow a reliable assignment of spectral properties to individual Chls. Attempts to use site-directed mutagenesis or single molecule spectroscopy have not been very successful for spectral/structural assignments so far, although promising first steps have been taken in both directions (Soukoulis et al., 1999; Jelezko et al., 2000). Thus, for the time being, simulations, in which the assignment of site energies to each of the Chls is treated as an adjustable parameter, are the method of choice. Nevertheless, with the new structure available a number of useful restrictions can be applied concerning the assignment of site energies (see below).

In this paper, we present the experimentally determined steady-state optical spectra (linear dichroism (LD), circular dichroism (CD), and absorption as function of temperature) and analyze them on the basis of the 2.5-Å structure by application of exciton coupling theory (Pearlstein, 1992). An approach introduced by Fetisova et al. (1996) allows one to study the excited state dynamics of this excitonically coupled system on the basis of Förster theory. We are thus able to simultaneously simulate both absorption and emission properties of PS I with a common set of site energies. This in turn opens the opportunity to use the set of optical spectra as a fitting criterion for the transition energies of the individual (noninteracting) Chls. Recently, this approach yielded convincing results for the FMO-complex (Owen and Hoff, 2001). Besides that, the limits of the excitonic coupling theory and its applicability for the description of the excitation transfer based on Förster theory are discussed and the consequences of the structural organization on the light harvesting process are studied in a quantitative way.

MATERIALS AND METHODS

Measurement of steady-state optical spectra

Trimeric PS I complexes were prepared from the thermophilic cyanobacterium *S. elongatus* as described by Fromme and Witt (1998). For absorption and CD measurements the concentrated samples were diluted to a final Chl concentration of ~10 μM with a buffer containing 20 mM Tricine (*N*-[2-hydroxy-1,1-bis(hydroxymethyl)ethyl]glycine, pH 7.5), 25 mM $MgCl_2$, 100 mM KCl, 5 mM sodium ascorbate, and 0.02% *n*-dodecyl-β-D-maltoside (β-DM). For measurements at cryogenic temperatures, glycerol was added to the samples to a final concentration of 65% (w/v). Absorption spectra were recorded with a spectral resolution of 1 nm on a Cary-1E-UV/VIS spectrophotometer, Varian, Darmstadt, Germany. CD spectra were measured with spectral width of 2 nm on a JASCO spectropolarimeter model J-720, Jasco, Gross-Umstadt, Germany.

For LD measurements, the samples were oriented by squeezing a 1.25 cm × 1.25 cm × 2 cm polyacrylamide gel along two perpendicular axes allowing it to expand in the third direction resulting in dimensions of 1.0 cm × 1.0 cm × 3.1 cm. The LD of the sample is defined as the difference in the absorption of light polarized parallel and perpendicular to the stretching direction of the gel. The light is propagating perpendicular to the stretching direction of the gel. The PS I complexes are disc shaped with two long axis parallel to the membrane plane and a short axis being the crystallographic C_3 axis (*z* axis in the 1JB0.pdb file), which is perpendicular to the membrane plane. Considering the shape of the PSI complexes they will align with their C_3 axis perpendicular to the stretching direction. The final composition of the gel was 14.5% acrylamide + 0.5% bisacrylamide in 20 mM Bis-Tris, 20 mM NaCl, and 0.02% ß-DM, at pH 6.5, polymerized with 0.06% *N,N,N′,N′*-tetra-methylethylenediamene, and 0.01% ammonium peroxodisulphate solution. LD spectra were recorded with a spectral resolution of 2 nm on a Beckmann DU 62 spectrophotometer, Bechman Coulter, Unterschleissheim-Lohof, Germany, using a film polarizer (Spindler and Hoyer model 10K, Göttingen, Germany).

For low temperature measurements, the cuvette was placed in a continuous flow helium cryostat (Oxford CF 1204, Wiesbaden, Germany) or liquid nitrogen bath cryostat (Oxford DN1704).

Structure-based calculation of distances, excitonic interactions, and transfer rates between Chls

All calculations were based on the published dataset of the x-ray structure of PS I from *S. elongatus* with 2.5-Å resolution (1JB0.pdb file; Jordan et al., 2001) containing the coordinates of 96 Chls and 22 Cars. For calculation of center-to-center distances *R* between Chl molecules, the arithmetic average of the coordinates of the four pyrrol nitrogen atoms have been used as the center of the Chl molecules, instead of the central Mg atoms, as those are located out of the ring plane of the Chls (by 0.35 Å on average). For calculation of closest contacts of the π systems R_π between different Chls, and between Chls and Cars, first the distances from any atom of the π-system of one molecule to any atom of the π-system of the other molecule (Fig. 1) were calculated and afterwards, the minimum of these values was selected, indicating the actual closest contact of the respective π-systems.

A structural factor s_{ij} was calculated using the center-to-center distances R_{ij} and the orientation factor κ as follows: $s_{ij} = \kappa_{ij}/R_{ij}^3$, in which κ is defined by $\kappa = (\hat{a} \cdot \hat{d}) - 3(\hat{a} \cdot \hat{R})(\hat{d} \cdot \hat{R})$, with $\hat{a}$ and $\hat{d}$ being unit vectors in the directions of the acceptor and donor transition dipoles and $\hat{R}$ in the direction of the line joining the dipole centers.

Förster transfer rates k_{ij} and excitonic coupling strengths J_{ij} between Chls *i* and *j* are calculated based on the structural factor s_{ij} as follows:

$$k_{ij} = s_{ij}^2 R_0^6/(0.667\tau) \quad (1a)$$

and

$$J_{ij} = 5.04\ \mathrm{C}\ s_{ij}\mu^2 \quad (1b)$$

The following values for the parameters are chosen: natural fluorescence lifetime $\tau = 15$ ns (Colbow, 1973), and oscillator strength of the Chl Q_Y (0–0) transition $\mu^2 = 21.5\ \mathrm{D}^2$ (Shipman, 1977). *C* takes into account the influence of the medium and is given by $C = (n^2 + 2)^2/9n^2$ (van Amerongen et al., 2000). Assuming $n = 1.5$ for the protein matrix, this gives $C = 0.89$. The Förster radius R_0 defines the distance for which the rate of energy transfer becomes equal to the intrinsic rate of radiative decay. For Chls with identical Q_Y transition energies ("isoenergetic"), a value of $R_0 = 74$ Å (Byrdin et al., 2000) has been used. The factor 0.667 in the denominator of Eq. 1a) corrects for the average κ^2 contained in R_0^6.

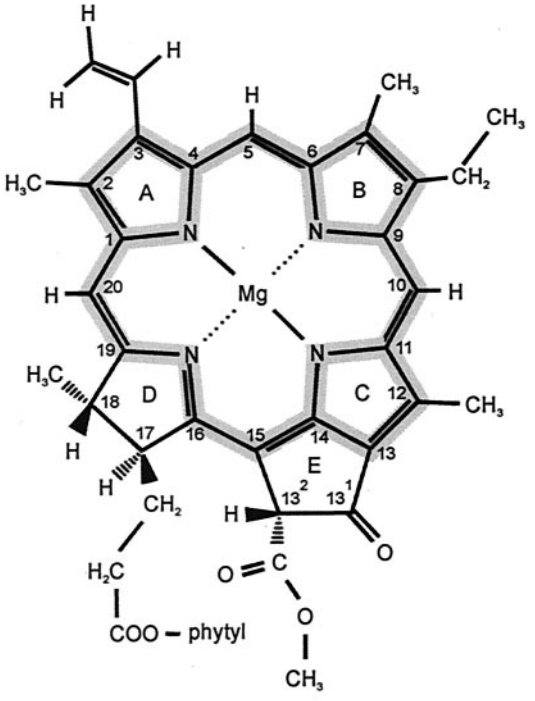

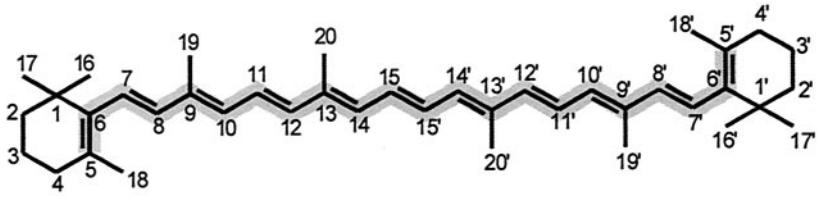

FIGURE 1 Molecule structure of Chl and Car. π-systems are shaded. In the Chl scheme, additionally the IUPAC ring nomenclature is indicated. The Q_Y transition moment lies approximately along the axis connecting the nitrogen atoms of rings A and C, respectively (van Amerongen et al., 2000).

Simulation of excitonic absorption, linear, and circular dichroism spectra

We analyze the experimental spectra with an excitonic model, which has been described previously, e.g., by Pearlstein (1992). The Hamiltonian of the system H is given by the coupling matrix containing all the 96×96 two-pigment coupling energies J_{ij}, and, on the main diagonal, the monomer transition energy of Chl i, ν_i. We diagonalize H to find its eigenvalues and eigenvectors. The thus defined transitions may differ in energy, direction, and oscillator strength from those of the individual noninteracting Chls. The energies ν_κ (in cm^{-1}) of the 96 all-complex exciton states are given by the eigenvalues of H. The components c_{iK} of the corresponding eigenvectors $c_K = (c_{1K}, \ldots, c_{iK}, \ldots, c_{96K})$ describe the contribution of pigment i to the exciton state K. Following Durrant et al. (1995) and Fidder et al. (1991), a delocalization parameter $N_K = 1/\Sigma_i(c_{iK})^4$ is calculated, which equals one for monomers, two for dimers, etc.

Steady-state optical spectra arising from excitonic coupling of all individual transition moments μ_i are calculated as follows (Pearlstein, 1992):

$$\text{Absorption: } \mu_K^2 = \sum_{i,j=1}^{96} \mu_i \mu_j (\hat{\mu}_i \cdot {}_j) c_{iK} c_{jK} \qquad (2a)$$

$$\text{CD: } \Re_K = 1.7 \times 10^{-5} \sum_{i,j=1}^{96} \nu \mu_i \mu_j R_{ij} [\hat{R}_{ij} (\hat{\mu}_j \times \hat{\mu}_i)] c_{iK} c_{jK} \qquad (2b)$$

$$\|\text{-Absorption: } \mu_{K,\|}^2 = \frac{1}{2} \sum_{i,j=1}^{96} \mu_i \mu_j [(\hat{\mu}_i \cdot \hat{\mu}_j) - (\hat{\mu}_i \cdot \hat{\varepsilon}) \times (\hat{\mu}_j \cdot \hat{\varepsilon})] c_{iK} c_{jK} \qquad (2c)$$

$$\perp \text{ Absorption: } \mu_{K,\perp}^2 = \sum_{i,j=1}^{96} \mu_i \mu_j (\hat{\mu}_i \cdot \hat{\varepsilon})(\hat{\mu}_j \cdot) c_{iK} c_{jK} \qquad (2d)$$

$$\text{LD: } LD_K = \mu_{K,\|}^2 - \mu_{K,\perp}^2 \qquad (2e)$$

Here μ_i^2 is the dipole strength of the transition moment on the ith molecule, $\hat{\mu}_i$ is the unit vector in the direction of that transition, c_{iK} is the ith element

of the eigenvector for the *K*th exciton state, v is the transition energy (in cm^{-1}), R_{ij} is the distance (in nm) from the center of the transition charge distribution of the *i*th molecule to that of the *j*th, $\hat{R}_{ij}$ is the unit vector in the direction of that vector, $\hat{\varepsilon}$ is the unit vector in the direction of the membrane normal (*z* axis). $\mu^2_{K,\perp}$ is the dipole strength of the component of the *K*th exciton transition moment perpendicular to the membrane plane, i.e., parallel to the membrane normal $\hat{\varepsilon}$. The membrane normal coincides with the crystallographic C_3 axis (see the trimerization axis in Fig. 4). $\mu^2_{K,\parallel}$ is the dipole strength of the component of the *K*th exciton transition moment parallel to the membrane plane. $\Re_K$ is the rotational strength of the *K*th exciton transition moment. Note, that the indices *parallel* and *perpendicular* refer to the membrane plane, which is oriented parallel to the stretching direction and not to the membrane normal $\hat{\varepsilon}$ entering Eqs. 2c and 2d.

For presentation, absorption, and linear dichroism stick spectra have been dressed by Gaussians with 360 cm^{-1} (~18 nm) full width at half maximum (FWHM), CD stick spectra, due to their narrowed nature, with 300 cm^{-1} (~15 nm) FWHM, and emission spectra with 400 cm^{-1} (~20 nm) FWHM. The amplitudes of these simulated spectra contain information on oscillator and rotational strength of the involved transitions.

Simulation of excitation energy transfer and trapping dynamics

The excited state dynamics of the PS I antenna-RC complex can be described by a set of coupled differential equations, the solution of which is found from the eigensystem of the system's 96 × 96 transfer matrix *T* (Byrdin et al., 2000). Consideration of excitonic coupling within the complex requires some modifications of *T* that are described below.

T is composed of transfer rates between pigments *i* and *j*, and on the main diagonal, depopulation rates. The transfer rate is the product of a structural factor, a spectral factor, and a scaling parameter defining the time axis. The structural factor k_{ij} is given by Eq. 1a and describes the transfer rate between Chls with identical transition energies, whereas the spectral factor is a normalized FOI between donor emission and acceptor absorption (for isoenergetic Chls FOI ≡ 1). For the calculation of the FOI, the Gaussian decomposition of the absorption spectrum of chlorophyll in diethyl ether by Shipman et al., 1976 has been slightly modified. The short-wavelength Gaussian corresponding to the 630-nm band has been slightly increased in amplitude and width with respect to the Q_Y (0-0) band to reproduce the spectral shape of Chl in micelles of ß-DM, which are expected to better mimic the biological membrane environment.

Chl emission spectra were obtained as mirror images of these absorption spectra. The differences to Chl emission spectra resulting from application of the Stepanov relation are negligible (compare Laible, 1995; Laible et al., 1998). A uniform Stokes shift of 130 cm^{-1} (~6.5 nm) has been used to ensure detailed balance (Laible, 1995; Laible et al., 1998). The depopulation rate k_i of the excited state *i* is calculated as $\sum_j k_{ij}$ with $j = 1, \ldots, 96$, in which k_{ii} is the rate for the intrinsic decay by fluorescence (0.5 ns^{-1} fixed) and, for both sites constituting P700, by charge separation (parameter k_{CS}). The inverse mean of all k_i is called "single step hopping time" and provides a measure of the connectivity between Chls within the PS I complex.

Lifetimes of excitation energy transfer and trapping processes τ_i have been determined from the eigenvalues of the transfer matrix *T*. The corresponding decay associated amplitudes result from the respective eigenvectors after weighting with the initial excitation distribution. Excitation was simulated as nonselective and stoichiometric, i.e., all pigments are excited with equal probability (except where otherwise indicated). A plot of the Gaussian dressed amplitudes weighted with the respective normalized oscillator strength versus the Stokes shifted transition energies of the states results in decay associated spectra (DAS). The steady-state emission spectrum is given by the lifetime weighted integral over all decay associated spectra and was calculated as $\sum_i \mathrm{DAS}_i \times \tau_i$. Of the 96 lifetime components obtained from the solution of the transfer equations, all with the exception of the very slowest few are characterized by lifetimes <2 ps and vanishing amplitudes. They mainly describe the exchange of excitation between spatially and/or spectrally neighboring states. Such processes are experimentally not resolvable, even with the high time resolution available at present. The spectrum resulting from summing up the spectra of all these processes is characteristic for very fast energy transfer processes in the bulk antenna directed towards thermal equilibration.

Alternatively, based on the transfer matrix *T*, Monte Carlo simulations of a random walk of the excitation through the complex have been performed. They resulted in essentially the same lifetimes but allowed in addition to follow the individual trajectory of the excitation.

The effects of excitonic coupling have been taken into account in the following way. The delocalized exciton states of strongly coupled (interaction energy >95 cm^{-1}) aggregates are regarded as donors and acceptors, respectively. All weaker couplings are neglected as being ruled out by the site inhomogeneities. Transfer rates from/to exciton sites have been calculated as described by Fetisova et al., (1996). In short, the structural factor s^2 is averaged over the s^2-factors of the exciton bands at the locations of the monomers and the FOI for the transfer from/to the exciton states are weighted with the normalized oscillator strength of the respective exciton band. To ensure fast thermal equilibration between exciton states, the relaxation rate from the higher exciton state has been set to 5 ps^{-1} and the reverse rate has been calculated from this according to Boltzmann. This results in an equilibration time between upper and lower exciton band of ~100 fs as found in the RC from purple bacteria (Vos et al., 1997) and PSII (Klug et al., 1998).

Thus, it becomes possible to simultaneously simulate all the spectral properties along with the excitation energy transfer kinetics of PS I based on a minimal set of common parameters consisting besides the two time scaling parameters (Förster radius R_0 for excitation transfer and primary charge separation rate k_{CS} for electron transfer) only of the assignment of transition energies to all the structurally defined Chls. As there are 96 of these, the parameter space appeared too multidimensional for a conventional fit routine. We therefore implemented a simulation program (in Mathematica 3.0) that uses the individual Chl transition energies as input values for the calculation of spectral properties and excitation transfer kinetics. Comparison of simulated and experimental optical spectra provided a criterion for the quality of the structural/spectral assignment. The assignment strategy was basically guided by symmetry relations, considerations regarding the axial ligands and H bonding to the Chls, functional arguments concerning the location of the red pigments (see below), and fine tuning of transition energies of the bulk pigments to improve the simulations of the optical spectra. The structural/spectral assignment thus determined (listed in Table 2) represents the distribution of transition energies that was found to agree best with the experimentally determined optical properties of the PS I complex.

We are aware of certain limitations of the applied simulation methods. For the sake of simplicity, the following assumptions have been made. 1) Dynamic disorder effects caused, e.g., by thermal fluctuations of Chl positions and orientations have been neglected. 2) Only Q_Y transitions have been taken into account, and possible influence of charge transfer interactions has been neglected. 3) The point dipole approach was used, although this approach may not be satisfactory where the distances between donor and acceptor are comparable with the size of the molecules (Table 3). Deviations between the interaction energies calculated by more accurate methods such as the transition monopole approximation (Chang, 1977) or the density cube method (Krueger et al., 1998) and the point dipole approach can be significant depending on the distance between the chromophores and the mutual orientation (see Appendix). However, given the lack of experimental data for the actual Coulombic interaction energies together with insufficient knowledge on the exact transition charge density distributions underlying these calculations, it appears hard to decide which of the various values is most appropriate. We therefore stick to the point dipole approach, which requires incomparably less computational efforts. 4) Above that, at distances between chromophores comparable with the van-der-Waals distance energy transfer based on the Dexter mechanism

TABLE 2 Position (A1, for example, is located in the stromal layer at 5 o'clock relative to the trimerization axis indicated by the black triangle (= 12 o'clock), see also Figs. 4 and 5), orientation (θ is the angle between the transition moment and the membrane normal), Q_Y transition energy (= color in nm), number (#) of and distance to the next carotenoid (Car), probability of being the last antenna Chl, which is visited before the excitation enters for the first time the RC calculated for homogeneous and heterogeneous site energies for the Chls in PS I (the asterisk indicates that these Chls belong to coupled aggregates if excitonic interactions >95 cm^{-1} are taken into account)

Chl	Layer/position	$\cos^2\theta$	Color [nm]	Next Car #	Distance to next Car [Å]	Last ant Chl [%] homogen/heterogen
A1	Stromal / 5	0.50	670	13	4.6	0.6 / 0.2
A2	Stromal / 5	0.57	670	13	7.8	0.2 / –
A3	Stromal / 4	0.00	680	3	11.7	0.1 / 0.2
A4	Middle / 4	0.02	675	3	6.7	0.3 / 0.1
A5	Lumenal / 5	0.25	665	12	4.3	0.3 / –
A6	Lumenal / 5	0.34	675	12	4.9	**1.3** / 0.1*
A7	Lumenal / 6	0.07	675	12	3.9	**1.4** / 1.1*
A8	Stromal / 4	0.11	665	3	11.6	0.1 / –
A9	Stromal / 5	0.04	665	13	13.9	0.1 / –
A10	Stromal / 4	0.14	672	3	6.4	– / – *
A11	Stromal / 4	0.45	670	3	6.6	– / –
A12	Lumenal / 4	0.48	670	2	3.6	– / –*
A13	Lumenal / 4	0.62	668	1	4.0	– / –
A14	Lumenal / 4	0.39	670	2	6.2	– / –
A15	Lumenal / 3	0.10	662	1	8.1	– / –
A16	Lumenal / 3	0.20	675	8	10.5	0.2 / –*
A17	Lumenal / 4	0.04	675	3	5.2	– / 0.1*
A18	Stromal / 4	0.49	672	1	4.4	– / –
A19	Stromal / 3	0.13	665	7	10.7	0.1 / –
A20	Stromal / 3	0.12	670	1	3.9	– / –
A21	Stromal / 3	0.02	670	7	8.5	0.1 / –*
A22	Stromal / 3	0.01	675	7	3.5	– / –
A23	Stromal / 3	0.08	675	7	5.8	0.3 / 0.1
A24	Middle / 3	0.74	679	8	3.6	**2.5** / 1.5
A25	Lumenal / 3	0.07	680	8	6.4	0.9 / 1.0*
A26	Lumenal / 4	0.24	675	11	4.8	**7.0** / 0.2*
A27	Lumenal / 4	0.24	675	3	4.5	0.4 / 2.8*
A28	Stromal / 4	0.13	665	8	11.4	**1.1** / 0.2
A29	Stromal / 2	0.25	679	7	7.7	0.7 / –*
A30	Stromal / 2	0.18	679	20	6.1	0.4 / 2.1*
A31	Middle / 1	0.64	675	20	3.9	**1.3** / –*
A32	Lumenal / 1	0.22	675	18	6.2	**3.4** / 2.0*
A33	Lumenal / 3	0.24	675	8	4.8	0.4 / –*
A34	Lumenal / 3	0.21	675	8	6.4	0.1 / 0.4
A35	Lumenal / 3	0.80	679	8	12.5	**1.8** / 1.2
A36	Lumenal / 2	0.87	680	20	13.0	**2.3** / –*
A37	Middle / 2	0.87	680	8	8.6	**3.7** / 9.1*
A38	Stromal / 7	0.04	694	14	5.2	**3.3** / 7.5*
A39	Stromal / 6	0.01	694	14	5.7	0.1 / 1.5*
A40	Middle / 6	0.97	701	11	5.1	**10.2** / 9.4
S1 (P700.A)	Lumenal / 3	0.21	683	11	13.6	
S2 (P700.B)	Lumenal / 2	0.26	683	17	16.8	
S3 (Acc.B)	Middle / 8	0.07	680	11	8.8	
S4 (Acc.A)	Middle / 2	0.04	680	17	11.1	
S5 (A_0.A)	Middle / 8	0.67	683	14	7.6	
S6 (A_0.B)	Middle / 2	0.60	683	17	6.9	
B1	Stromal / 11	0.44	675	21	4.5	0.2 / –
B2	Stromal / 10	0.02	680	21	9.4	0.2 / 0.2
B3	Middle / 11	0.00	675	5	6.7	0.5 / 0.1
B4	Lumenal / 11	0.24	665	18	6.2	0.2 / –
B5	Lumenal / 11	0.39	695	17	6.3	**1.1** / 1.4
B6	Lumenal / 12	0.35	706	17	5.9	**2.3** / 2.6
B7	Lumenal / 12	0.00	712	18	4.0	0.8 / 2.6

Continued

TABLE 2 Continued

Chl	Layer/position	$\cos^2\theta$	Color [nm]	Next Car #	Distance to next Car [Å]	Last ant Chl [%] homogen/heterogen
B8	Stromal / 11	0.09	660	5	9.0	0.1 / –
B9	Stromal / 10	0.14	672	5	5.2	– / –
B10	Stromal / 10	0.46	670	5	5.2	– / –
B11	Lumenal / 10	0.51	675	6	3.6	– / –
B12	Lumenal / 10	0.67	675	4	4.3	– / –
B13	Lumenal / 9	0.08	665	4	7.4	– / –
B14	Lumenal / 9	0.19	675	10	11.2	0.2 / –*
B15	Lumenal / 10	0.08	675	5	8.4	0.1 / 0.1*
B16	Stromal / 9	0.19	665	9	9.6	– / –
B17	Stromal / 10	0.41	672	4	4.5	– / –*
B18	Stromal / 9	0.08	670	4	4.0	– / –
B19	Stromal / 9	0.02	670	9	5.5	– / –*
B20	Stromal / 9	0.00	675	9	3.5	– / –
B21	Stromal / 9	0.05	675	9	7.2	0.1 / 0.1
B22	Middle / 9	0.78	679	10	3.8	**3.3** / 2.4
B23	Lumenal / 9	0.13	680	10	5.7	0.7 / 0.8*
B24	Lumenal / 10	0.16	675	5	11.9	**6.8** / 0.3*
B25	Lumenal / 10	0.24	675	5	5.2	0.4 / 2.7*
B26	Stromal / 10	0.15	665	10	12.4	**1.4** / 0.2
B27	Stromal / 8	0.21	679	9	5.1	0.7 / –*
B28	Stromal / 8	0.17	679	16	3.6	0.4 / 1.8*
B29	Middle / 7	0.42	675	14	4.0	**1.8** / –*
B30	Lumenal / 6	0.44	675	12	4.6	**2.9** / 3.4*
B31	Lumenal / 9	0.25	670	10	4.6	0.3 / –*
B32	Lumenal / 9	0.15	670	10	7.1	0.1 / 0.5*
B33	Lumenal / 9	0.03	670	10	13.1	0.1 / –*
B34	Lumenal / 8	0.77	679	10	10.9	**1.6** / 1.5
B35	Lumenal / 8	0.85	680	15	4.5	**2.2** / –*
B36	Middle / 8	0.84	680	9	6.3	**4.5** / 10.2*
B37	Stromal / 1	0.03	694	17	5.0	**2.0** / 4.0*
B38	Stromal / 1	0.03	694	17	5.5	0.1 / 1.6*
B39	Middle / 1	0.92	702	17	3.6	**18.0** / 21.6
J1	Middle / 6	0.83	674	14	3.8	0.3 / 0.2
J2	Lumenal / 6	0.51	677	13	4.2	0.1 / –
J3	Lumenal / 7	0.58	668	15	3.8	0.1 / –
K1	Lumenal / 3	0.00	666	1	12.2	– / –
K2	Middle / 3	0.61	670	2	6.7	– / –
L1	Stromal / 12	0.13	665	20	11.5	0.1 / –
L2	Stromal / 1	0.73	716	19	4.2	0.3 / 0.2
L3	Lumenal / 1	0.12	700	20	9.8	0.4 / 0.1
M1	Stromal / 11	0.88	674	22	10.1	– / –
X1	Middle / 8	0.35	660	16	4.3	0.2 / –
P1	Stromal / 2	0.00	702	7	4.9	0.1 / 0.3

Further details see text.

(Dexter, 1953) may become relevant, which was also excluded from consideration here.

RESULTS AND DISCUSSION

Steady-state absorption spectroscopy of the PS I complex

Previously reported spectroscopic data for PS I from *S. elongatus* (e.g., Pålsson et al., 1998) have been complemented by steady-state absorption measurements as a function of polarization and of temperature to obtain additional information to what extent excitonic interactions contribute to the spectral properties. Fig. 2 shows the absorption spectra of the PS I complex from *S. elongatus* at 5, 80, 160, 220 K, and at room temperature (RT).

Besides the broad main peak centered at ~680 nm additional spectral features can be distinguished in the long wavelength region. A shoulder observed at ~710 nm at higher temperatures is resolved as a separate peak at lower temperatures. Generally, the low temperature spectra show distinctly more structured features than the spectra above 100 K. Both on the short- and on the long-wavelength side

TABLE 3 Characteristics of the strongest coupled dimers in PS I: excitonic interaction energy calculated in the point dipole approximation ($J < 0 \Rightarrow$ sum band (Σ) lies energetically lower), cosine of the angle β between the transition dipoles, ratio of the oscillator strength ($\cos\beta < 0 \Rightarrow$ less oscillatory strength in the sum band), center-to-center and edge-to-edge distance and excitonic interaction energy calculated in the extended dipole approximation

Chl *a* dimers	Excitonic coupling J [cm^{-1}] (point dipole approx.) (band positions calculated with monomeric transition energies as in Table 2 [nm])	Cos of the angle between the transition dipoles	Ratio of oscillator strength (Σ/Δ)	Distance between ring-centers [Å]	Edge-to-edge distance [Å]	Excitonic coupling J [cm^{-1}] (extended dipole)
S1-S2	414.8 (664/703)	−0.53	0.31	5.76	3.57	138.3
B31-B32	−247.7 (681/659)	0.99	190.8	8.29	3.50	−252.0
B32-B33	−241.8 (681/659)	0.97	75.9	8.03	3.80	−203.6
A12-A14	−230.9 (681/660)	0.99	288.8	8.35	3.73	−218.1
A32-B7	210.9 (673/715)	−0.83	10.6	8.89	3.45	244.4
B37-B38	−205.7 (704/684)	−0.63	0.22	7.51	3.61	−172.1
S4-S6	189.4 (690/673)	−0.33	0.50	7.75	3.64	141.6
A10-A18	−180.6 (680/664)	0.86	13.2	9.11	3.79	−190.4
B9-B17	−179.4 (680/664)	0.89	16.7	8.74	4.03	−160.9
A38-A39	−167.8 (702/686)	−0.71	0.17	7.97	3.59	−145.7
A33-A34	−162.4 (682/668)	0.87	14.3	9.85	3.70	−193.8
S3-S5	157.4 (689/674)	−0.34	0.49	8.29	3.83	130.5
A31-A32	145.8 (668/682)	−0.90	0.05	9.92	3.75	158.5
A36-A37	−141.0 (687/674)	0.99	289.3	10.21	3.64	−158.9
A26-A27	−138.4 (681/669)	−0.20	0.67	9.14	4.83	−135.1
B24-B25	−134.9 (681/669)	−0.18	0.69	9.04	4.85	−129.5
A20-A21	−131.6 (676/664)	0.97	65.2	10.10	4.12	−135.4
B18-B19	−124.0 (676/664)	0.91	21.3	10.28	4.16	−129.2
B14-B15	−122.5 (681/669)	−0.17	0.72	9.25	4.77	−120.6
A16-A17	−120.9 (681/670)	−0.15	0.74	9.24	4.72	−120.6
B27-B28	−120.9 (685/673)	0.99	378.4	10.35	4.16	−123.2
B35-B36	−120.1 (686/674)	0.98	105.4	10.53	3.97	−127.8
A16-A25	−113.3 (672/683)	0.97	14.9	10.84	4.40	−123.7
A29-A30	−110.8 (684/674)	0.96	51.9	10.12	4.24	−99.9
A7-A6	−108.8 (680/670)	0.81	9.5	10.62	4.13	−112.8
B29-B30	103.0 (670/680)	−1.00	0	11.62	4.45	120.7
B14-B23	−96.8 (672/683)	0.99	389.6	11.38	4.67	−103.8
S1-S3	−92.1 (687/676)	0.50	2.98	11.90	4.72	−104.8
S2-S4	−87.0 (686/677)	0.55	3.44	12.14	4.91	−98.8

Pairs of Chls with nonparallel transition moments are shaded.

of the main peak separate features begin to emerge with decreasing temperature. Three "isosbestic" points can be distinguished at 657, 688, and 705 nm. Whereas the total area enclosed by the spectra stays essentially constant, a considerable redistribution of absorption can be noticed. Especially pronounced is the absorption increase with decreasing temperature in the red region above 705 nm at the expense of the 688- to 705-nm region. A weaker effect is observed on the blue side of the main peak: the area in the region between 657 and 688 nm increases at the expense of the region <657 nm upon lowering the temperature. Fig. 2 shows unambiguously that the amount of long wavelength absorption in the complex is temperature dependent. Such redistribution of absorption as a function of temperature has been found also for PS I from *Synechocystis* sp. (Rätsep et al., 2000) and *Spirulina* pl. (Cometta et al., 2000). It may be explained by an appropriate temperature dependence of the dielectric constant ε of the protein environment. Charge transfer interactions could be involved as well (Beekman et al., 1997; Rätsep et al., 2000).

Fig. 3 shows polarized steady-state spectra of the PS I complex from *S. elongatus*. In Fig. 3 *a* the LD spectrum at RT is presented. For comparison, the absorption spectrum is also plotted as a dashed line. Note the different ordinate scales for the two curves. Linear dichroism spectra display the difference in absorption of light polarized parallel and orthogonal to the stretching direction of the gel. Due to the shape of the PS I complexes, they will align with their C_3 axis perpendicular to the stretching direction (see Materials and Methods). The C_3 axis is parallel to the membrane normal $\hat{\varepsilon}$ and has been chosen as *z* axis in the 1JB0.pdb file. Chlorophylls oriented in the PS I complex with their transition moments parallel to $\hat{\varepsilon}$ will absorb incident light polarized orthogonal to the stretching direction of the gel. On average, one-half of the chlorophylls with transition moments lying in the membrane plane will absorb incident light polarized parallel to the stretching direction.

The maximal amplitude of the observed LD (Fig. 3 *a*) is approximately one-tenth of the total absorption, small negative amplitudes are observed at wavelengths <665 nm.

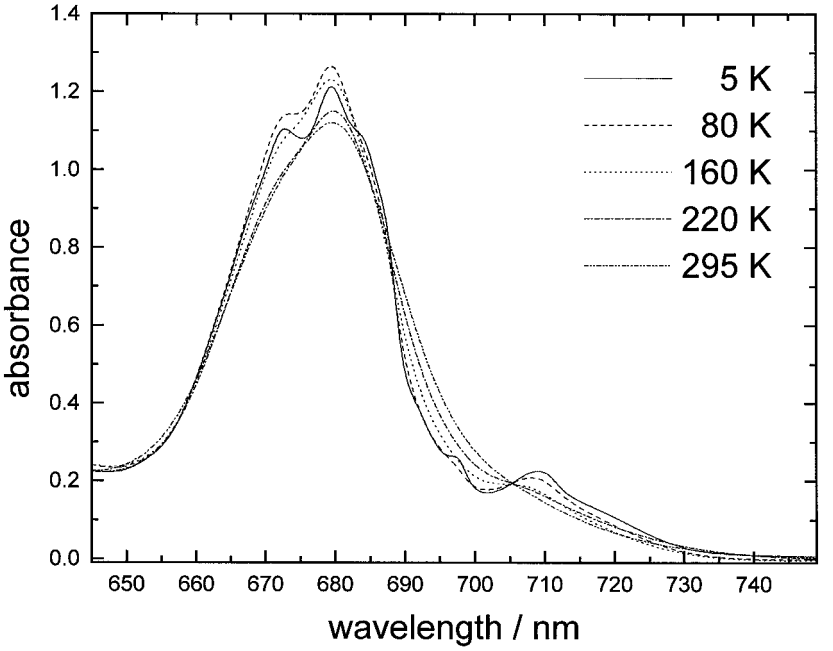

FIGURE 2 Steady-state absorption of the trimeric PS I core complex from *S. elongatus* at various temperatures. Note the "isosbestic" points at 657, 688, and 705 nm, and the redistribution of oscillator strength into the red with decreasing temperature.

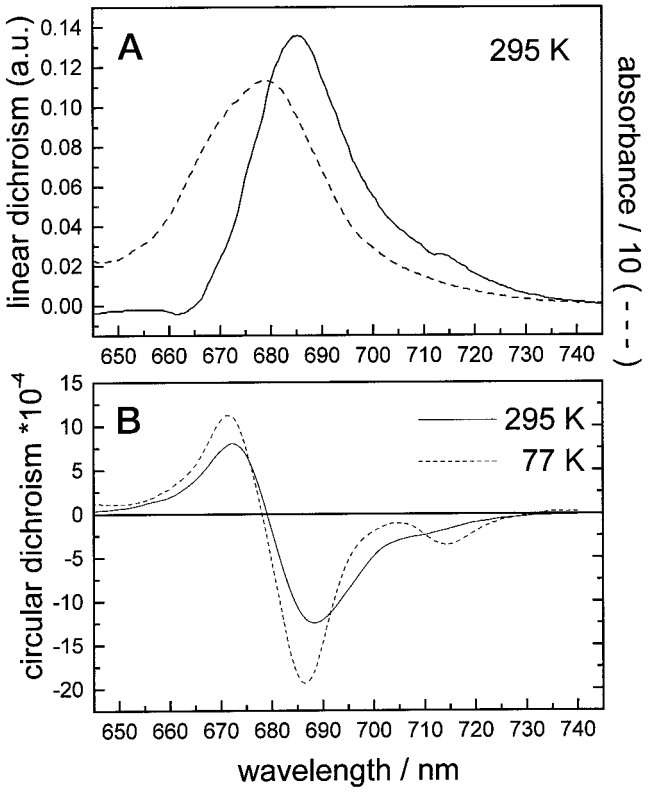

FIGURE 3 Steady-state polarized absorption of the trimeric PS I complex from *S. elongatus*. (*a*) Linear dichroism (*solid*) at RT, for comparison the nonpolarized absorption from Fig. 2 (divided by 10) is shown as well (*dashed*). (*b*) Circular dichroism at RT (*solid*) and at 77 K (*dashed*). Note that only at the red side a separate peak appears at low temperature.

Hence, for the latter spectral region, absorption due to transition moments with preferential orientation parallel to the membrane plane are quite well compensated by absorption due to transition moments oriented perpendicular to the membrane plane. In contrast, for longer wavelengths there is an excess of parallel absorption. The maximum of this positive LD is reached at ~685 nm, i.e., 5 nm to the red of the absorption maximum. This shows that transitions at longer wavelengths lie, in tendency, parallel to the membrane plane. The contribution of the 96 Chls to the LD signal is given by the squared cosine of the angle θ between the transition moment and the membrane normal $\hat{\varepsilon}$ (see column 3 of Table 2). Fig. 3 *b* shows the CD spectra of the PS I complex from *S. elongatus* at 77 K and at RT. The $CD = A_L - A_R$ at low temperature is larger than that at RT. Both spectra exhibit the positive lobe on the high energy side. The areas enclosed by the two lobes of each spectrum and the *x* axis are not equal, a phenomenon referred to as nonconservativity. In our case, the area of the negative lobe is about twice that of the positive one. Interestingly, the redistribution of absorption to the red with decreasing temperature found in the absorption spectrum (Fig. 2) is observed in the CD spectrum as well (compare the position of the side band in the 77-K spectrum and that of the shoulder in the RT spectrum in Fig. 3 *b*.) Note that the emergence of a separate peak with decreasing temperature is observed only on the low-energy side of the spectrum. This feature can be attributed to the low exciton band of coupled Chls giving rise to long wavelengths absorption. The corresponding CD from the high energy exciton band seems obscured by the main positive peak. Finally, the blue shift of the zero-crossing point with decreasing temperature is notewor-

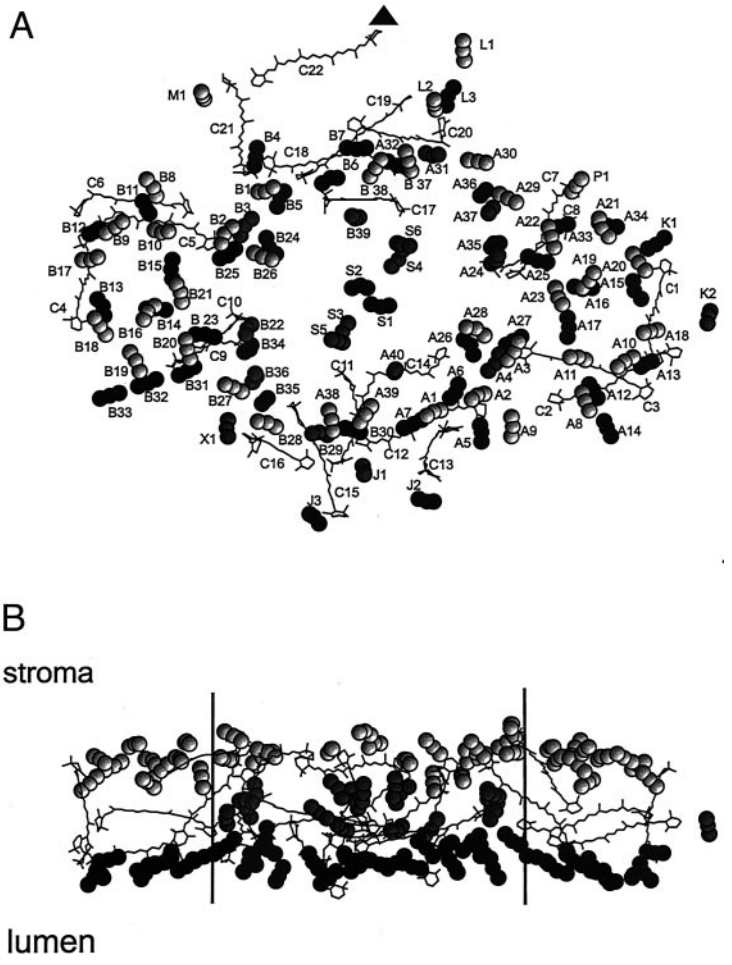

FIGURE 4 Arrangement of the pigments within the PS I complex from *S. elongatus* (*a*) top view, (*b*) side view; carotenoids are shown completely and marked with a capital C, Chls are represented by three atoms: the central magnesium and two nitrogens. The connecting line between the nitrogens defines the direction of the Q_Y transition dipole. The coding by different shades of gray means: light gray-stromal, dark gray-membrane buried, black-lumenal. Chls are marked by the letter of the binding subunit and a running number. The trimerization axis is on top (*black triangle*). The six Chls in the center belong to the RC, the rest to the core antenna. The two vertical lines in *b* indicate separation of antenna Chls coordinated by PsaA/B into a central part and peripheral parts as suggested by Jordan et al. (2001).

thy. CD spectra for other cyanobacteria have been presented by van der Lee et al. (1993) at 77 K for *Synechocystis* and at RT by Cometta et al. (2000) for *Spirulina* pl. Both of these spectra are similar to the ones presented here: smaller positive lobe on the high-energy side and larger negative lobe on the low-energy side.

Structural organization of the PS I complex from a functional point of view

Structural elements of the light harvesting antenna

In the following, we describe the arrangement of the Chls and Cars based on the recently published 2.5-Å structure of PS I from *S. elongatus* (Jordan et al., 2001). Fig. 4 shows the pigment arrangement of one monomeric unit of the trimeric PS I complex in two projections: 1) view from the top onto the membrane plane and 2) view from the side along the membrane plane. In Fig. 4 *a* the complex is shown with the trimerization axis on top (black triangle). In Fig. 4 *b* the same complex is shown with the view direction parallel to the membrane plane; PsaJ and PsaF are in front, PsaL and the trimerization domain are on the backside.

The carotenoids are shown with their whole carbon backbone; the chlorophylls are represented by just three atoms per molecule: the central magnesium and two nitrogen atoms. The connecting line between these nitrogens defines the direction of the Q_Y transition moment. All the carotenoids are labeled by a capital C and numbered from 1 to 22 (corresponding to BCR 4001 to BCR 4022 in the 1JB0.pdb file). The labels of the chlorophylls consist of a capital letter indicating the protein subunit coordinating them followed by a number. The numbers refer to the order of the Chl ligands along the polypeptide chain and increase from the N to the C terminus. Exceptions are the Chls belonging to the RC (S1 to S6), which are bound by PsaA/PsaB (see Table 2) and the Chl P1, which is coordinated by a phospholipid.

The top view onto the PS I complex (Fig. 4 *a*) shows that the six RC pigments are well separated from the surrounding antenna Chls. The Chls are coded by different shades of gray according to the *z* coordinates of the central Mg atoms reflecting their membrane depth, as follows: light gray, stromal ($z < 72$ Å); black, lumenal ($z > 81$ Å); and dark gray, in the middle of the membrane. The side view (Fig. 4 *b*) reveals that 79 of all identified Chls are located near the

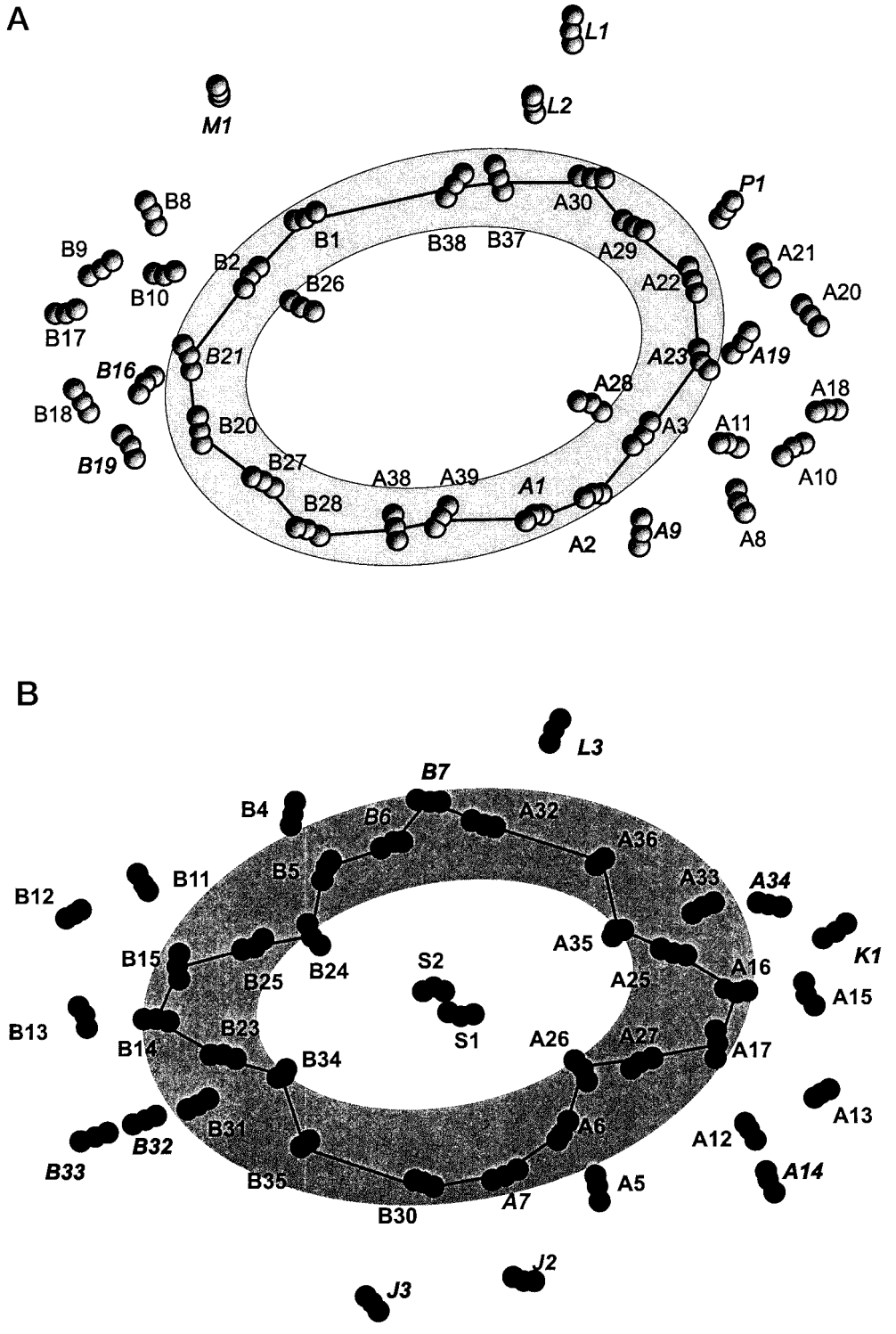

FIGURE 5 Top view of separate Chl layers (*a*) stromal, (*b*) lumenal; coding as in Fig. 4. Chls indicated in *Italics* have no symmetric counterpart on the respective other protein subunit.

stromal (top, light gray) and lumenal (bottom, black) membrane surface, respectively. The vertical lines in Fig. 4 *b* indicate the separation into a central and two peripheral parts as proposed by Jordan et al. (2001).

Fig. 5 shows separately the Chls of the two layers: stromal (light gray) in Fig. 5 *a* and lumenal (black) in Fig. 5 *b*. The Chls closest to the center are located within elliptical rings with half axes of ~25 and 40 Å and a width

of ~15 Å (shaded in Fig. 5). Lines connect neighboring Chls in the shaded rings. Note that four Chls of the stromal and six Chls of the lumenal rings belong to the peripheral part of the antenna system, which is thereby connected to the central part. The lumenal and stromal Chl rings are slightly twisted against each other (see Fig. 4 *a*). The distorted ring-shaped arrangement of the Chls in PS I obviously differs from the highly ordered and symmetric ring structure established for the LH2 antenna complex of purple bacteria (McDermott et al., 1995; Koepke et al., 1996), although dimensions (~2.5 nm), number of (bacterio)Chls (16-22) and the distances between neighbors within the rings (0.9–1.1 nm) are similar. In the purple bacterial system, the rings arise from highly symmetric protein structures, which are not found in the case of the PS I antenna. As a consequence, all Chls of the PS I rings have different orientations and a much lower symmetry is observed. Nevertheless, in the following, this distorted elliptical arrangement will be referred to as ring. The common ring arrangement in the two types of antennae rather indicates functional similarity than common ancestors for the PS I core antenna and LH2. The antenna is extended by two groups of Chls to the right and to the left of the lumenal and stromal Chl rings. Additionally, some Chls (e.g., M1, J2, J3, K2, and L1) are located rather isolated. Chlorophylls bound by the PsaA and PsaB subunits are usually related by the PsaA/B pseudo-C_2 symmetry. The interface between the PsaA and PsaB subunit is approximately defined by the plane connecting the four RC pigments S3–S6. Major deviations from this C_2 symmetry are found in the lumenal layer: no counterparts exist for the B31/32/33 trimer, the A33/34 and A12/14 dimers, and certain single chlorophylls. Two other deviations may be functionally relevant: Chl A1 has no symmetry analogue bound by PsaB and Chl B7 has no symmetry analogue bound by PsaA. The presence of B7 in the lumenal ring between A32 and B6 gives rise to the strongest coupled four-pigment-cluster found in the PS I complex: A31-A32-B7-B6 with coupling strengths of 146 cm^{-1}, 211 cm^{-1}, 79 cm^{-1}, respectively. The correspondence between the stromal and lumenal rings is disturbed at the 6 and 12 o'clock positions (see Fig. 5), where to each of the single lumenal Chls (B30, A32) corresponds a pair of stromal Chls (A38/39, B37/38). These pairs of Chls on the stromal side, A38/39 and B37/38, are in close proximity to the so-called "linker" Chls A40 and B39 and will therefore be named linker dimers. We will refer to the aggregate of one linker dimer and the corresponding linker Chl as linker cluster. Because the linker Chls are closest to the RC cofactors of all antenna Chls, it has been suggested early on that the energy transfer from the antenna into the RC proceeds through them (Schubert et al., 1997). This suggestion is challenged by the fact that the distance of the Chls in the linker clusters to all other antenna Chls is rather large.

Network of energy transfer pathways

The rates of pairwise energy transfer depend on distance and orientation factor between pigments, which became available with the improved structural resolution (Jordan et al., 2001). Based on this, excitation transfer rates have been calculated assuming uncoupled Chls of identical transition energies and a Förster radius of $R_0 = 7.4$ nm. Fig. 6 depicts pathways of fast energy transfer between Chls. All rates >0.3 ps^{-1} (which corresponds to a transfer step faster than one-tenth of the trapping lifetime) are represented by lines connecting the transfer partners. The thickness of the connecting lines increases with increasing transfer rates: 0.3–3 ps^{-1}, thin lines; 3–11 ps^{-1}, medium lines; >11 ps^{-1}, thick lines. Together, these rates cover >97% of the sum of all rates. Remarkably, a single network of energy transfer pathways is formed including all the Chls (with the exception of M1, see below). The scheme is based on Fig. 4, emphasizing the structural elements discussed above with corresponding shading code. For clarity, the lumenal ring and the stromal ring are displayed as an outer ring in dark gray and an inner ring in light gray. Chls in the middle of the membrane are shown between the rings in medium gray, except for the RC Chls, which are presented in the center. The remaining peripheral Chls have been placed outside the outer ring.

Excitonic coupling between closely packed neighboring Chls leads to an altered orientation of transition moments and thus modifies transfer rates. Increased rates are represented by wavy lines and decreased rates are represented by broken lines. Fig. 6 shows that excitonic coupling is essential to attain high transfer rates along the rings. In the lumenal ring, e.g., the orientation factor of A27 with respect to A17 is so poor ($\kappa^2 = 0.12$), that hardly any energy transfer would be possible without excitonic coupling. The same is true for B15-B25 ($\kappa^2 = 0.17$), A26-A6 ($\kappa^2 = 0.014$), and B24-B5 ($\kappa^2 = 0.024$). In these cases, high transfer rates are achieved due to excitonic coupling of Chls A26/27 and B24/25, respectively. The resulting excitonic transition moments are oriented in a way that gives favorable values for the orientation factor with respect to their neighbors ($\kappa^2 \sim 1$). The same mechanism applies to the connection of the linker dimers (A38/39, B37/38) to the rest of the antenna. Nevertheless, due to the missing symmetry analogue of A1, the stromal ring is interrupted between B37/38 and B1. In this context it is interesting to note, that in all cases, where the transfer rates between neighbors within the ring are rather small (e.g., A32-A36, B30-B35), the lumenal and stromal rings are connected to each other via fast energy transfer pathways involving the membrane embedded Chls A4, A31, A24 via A37, B3, B29, and B22 via B36. The four major connections between the two rings are emphasized by shading in Fig. 6. Thus, the central part of the network, constituted by the stromal and lumenal rings together with the bridges between them, surrounds the RC

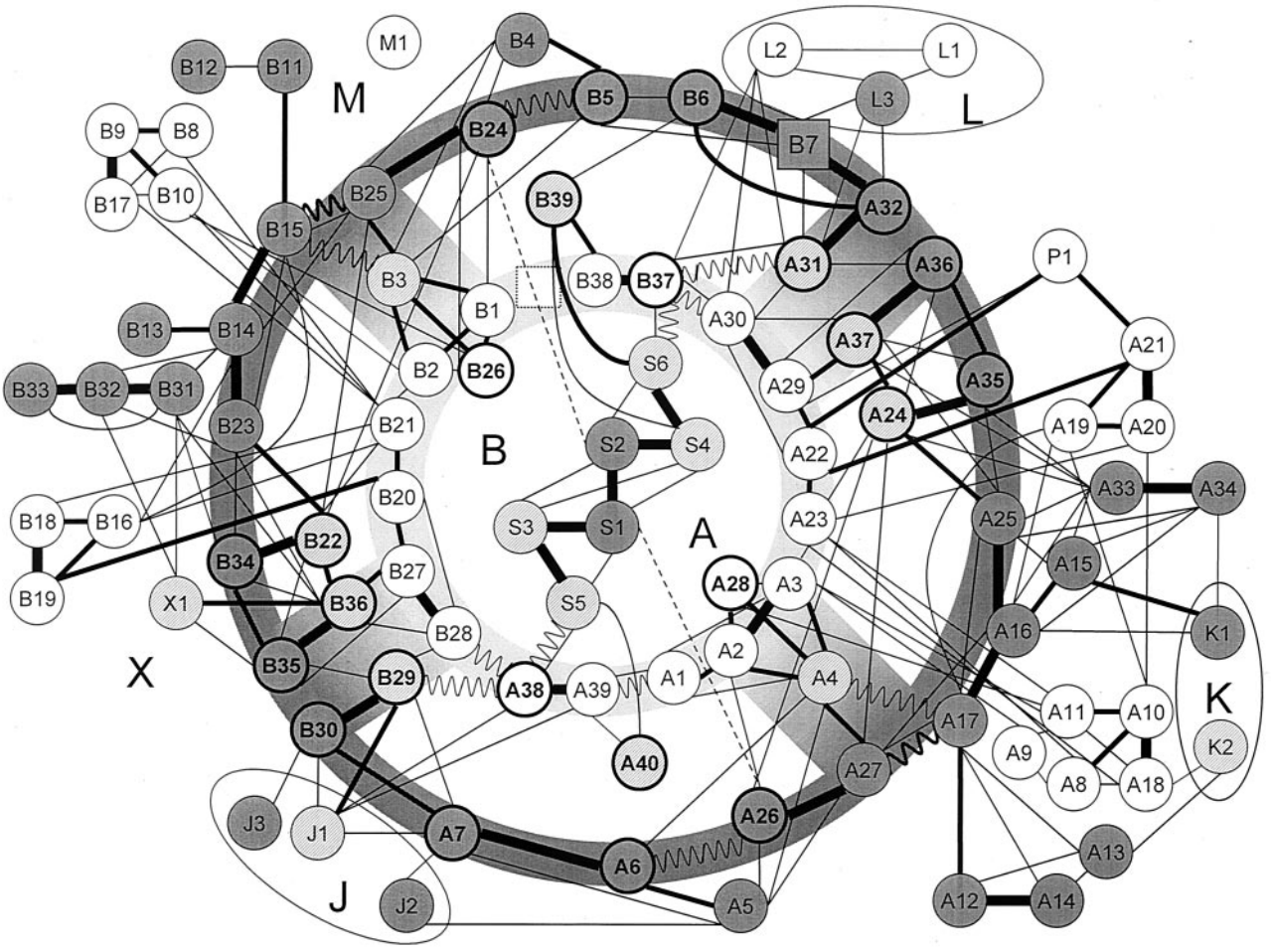

FIGURE 6 Scheme of energy transfer pathways within the PS I complex from *S. elongatus*. For clarity, the lumenal ring and the stromal ring are displayed as an outer ring in dark gray and an inner ring in light gray. Chls in the middle of the membrane are shown between the rings in medium gray, with the exception of the Chls in the RC, which are presented in the center. The remaining peripheral Chls have been placed outside the outer ring. All transfer rates $>0.3\ ps^{-1}$ are shown; line thickness encodes transfer speed: thin, 0.3 to 3 ps^{-1}; medium, 3 to 11 ps^{-1}; thick, $>11\ ps^{-1}$; wavy lines indicate enhancement of transfer rates via modified orientation by excitonic interaction, dashed lines show reduction of transfer rates by the same mechanism. Chls in bold type are visited last with a probability of $>1.0\%$ before the excitation enters the RC for the first time. Squares instead of circles indicate major symmetry breakings between PsaA and PsaB.

pigments like a shell. The two groups of Chls that extend the antenna to the left and right of the lumenal and stromal rings are well connected to this shell via multiple pathways. As a consequence, the central part of the network can be reached from any Chl in no more than three steps. This is also valid for all of the above mentioned rather isolated Chls with one exception. Chl M1 is only in weak contact with B8 but is better connected to Chls of the adjacent monomer of the trimeric PS I complex. It could play a role in excitation energy exchange between the monomers of a trimer.

To follow the migration of an individual excitation through the network to P700, Monte Carlo simulations have been performed for both a spectrally homogeneous antenna (all Chls isoenergetic and not excitonically coupled) and a spectrally heterogeneous antenna of excitonically coupled Chls using the spectral assignment derived below (see "color" column of Table 2). We analyzed statistics of twenty-thousand excitations. They revealed that the number of steps an excitation undergoes before it is trapped in the RC can be several hundreds (on average 1250/173 for spectrally homogeneous/heterogeneous antenna). During this walk it migrates randomly through the antenna system and changes back and forth between the stromal and lumenal layers several times (79/42 Chls are visited on average). The RC can also be entered and left several times (16/6 on average), before charge separation takes place. The last antenna Chl, which was visited before the excitation energy enters for the first time the RC, was registered. The results (in percent) are listed in the last column of Table 2.

For a spectrally homogeneous antenna, the 24 Chls registered more often than 1.0% of the total are marked by bold circles in Fig. 6. Altogether they represent more than 85%

of all last visits. Most of them are located in the lumenal ring. 28.2% are allotted to the two linker clusters, i.e., the excitation energy is channeled into the RC to a large extent via the linker clusters. However, the larger part (71.8%) is transferred via all the other Chls. Only the 23 most outlying Chls hardly contribute to the transfer to the trap ($<0.1\%$, compare also Table 2).

Summarizing, all chlorophylls are part of a well-organized network of energy transfer pathways. This arrangement suggests that excitation energy is distributed extremely fast over the whole complex due to the efficient transfer rates between neighboring Chls. This may explain the observed short lifetimes of excitation energy equilibration processes in the bulk antenna (see Introduction).

Within the network, most of the Chls are connected to at least four (4.5 ± 1.7 on average) neighbors by rates >0.3 ps^{-1}, which corresponds well to the number of direct neighbors within a two-dimensional square lattice. This illustrates the fact, that all ring Chls are additionally in contact with Chls embedded within the membrane, thereby constituting connections to the opposite layer, or with peripheral Chls. Only Chls B11/B12 and J3 are connected to the network only via a single channel. The otherwise multiple connections may provide an increased robustness with respect to possible local perturbations.

The antenna network is connected to the RC via multiple pathways on all three levels: lumenal (whole ring, especially A26/27, B24/25), inner-membrane (A24, A31, A37, B22, B29, B36), and in particular, stromal and inner-membrane by the linker clusters (A38/39/40, B37/38/39). Note that multidirectional energy transfer between the antenna and the RC has been recognized as a key feature for efficient light harvesting in purple bacteria (Schulten, 1999; Sundström et al., 1999).

Excitonic interaction in the PS I complex

Modeling optical spectra of PS I at 295 K taking into account excitonic interactions

Previous attempts to describe the absorption of the PS I complex were based on a decomposition of low-temperature spectra into various Gaussian bands associated with various "spectral pools" (e.g., Karapetyan et al., 1997; Byrdin et al., 2000; Gobets et al., 2001). This approach is at odds with the temperature dependence of the absorption spectrum (Fig. 2). Furthermore, the recently determined x-ray structure (Jordan et al., 2001) clearly shows that excitonic interactions (compare Table 3) between Chls cannot be neglected. In the following we describe an approach to simulate simultaneously absorption, transfer, and emission spectra of the PS I complex taking into account excitonic interactions between Chls.

For excitonically coupled dimers, the new (excitonic) transition moments are given by the vector sum (Σ) and difference (Δ) of transition moments of the uncoupled monomers and are oriented perpendicular to each other, accordingly. The energy splitting is twice the excitonic interaction energy J. The distribution of the oscillator strength over these two exciton bands depends on the angle between the transition moments of the monomers, whereas the sign of the interaction energy (i.e., whether the excitonic band related to the vector sum is higher or lower in energy) depends also on the angles between the transition moments of the monomers and the vector connecting them (see Materials and Methods and Table 3).

Calculation of the interaction energies (according to Eq. 1b) shows that more than one-half of the chlorophylls are involved in excitonic couplings exceeding 100 cm^{-1}, corresponding to 200 cm^{-1} ($\sim$10 nm) band splitting. Properties of Chl dimers with $J > 100$ cm^{-1} are listed in Table 3. For most of the strongly coupled dimers the monomer transition dipoles are nearly parallel oriented (see the columns 3 and 4 of Table 3). In these cases, virtually all oscillator strength is concentrated in the red shifted lower excitonic band. However, eleven pairs of Chls with nonparallel transition moments can be found (shaded in Table 3). For A16-A17, A26-A27, B14-B15, B24-B25, and the linker dimers A38-A39, B37-B38, this might be functionally relevant in terms of efficient energy transfer (see above). For the five dimers within the RC, the (more or less) even distribution of oscillator strength over the excitonic bands provides better spectral overlap to the antenna. The strongest coupling is found between the two pigments constituting the special pair of P700 with 415 cm^{-1}, corresponding to an excitonic splitting of $\sim$39 nm. Prominent aggregates of strongly coupled Chls include the trimer B31-B32-B33 and the tetramer A31-A32-B7-B6.

Fig. 7 demonstrates the effects of the excitonic interactions on the absorption spectrum of PS I. Fig. 7 *a* shows the experimental absorption spectra of the trimeric PS I complex from *S. elongatus* in the Q_Y region (dash-dot) and the absorption of Chl *a* in 80% (v/v) acetone/water (solid). The absorption of Chl *a* in the PS I protein complex is both broadened and red-shifted with respect to that of Chl *a* in organic solvents. Fig. 7 *b* shows a Gaussian band intended to represent the Q_Y absorption band of 96 spectrally identical Chls with no excitonic coupling (solid). For the sake of simplicity, a single Gaussian has been used and absorption on the short wavelength side of the Q_Y band due to Q_X (0-0) and Q_Y (0-1) transitions has been neglected. Accordingly, the experimental spectra have been corrected by subtracting the 630-nm band (and its mirror image from the emission data, respectively). The band width (FWHM = 18 nm) has been chosen as observed for Chl *a* in organic solvent (Seely and Jensen, 1965). The excitonic interactions between all 96 Chls give rise to a broadening of the absorption band and a red shift of the absorption maximum (see dashed line in Fig. 7 *b*). The absorption maximum of the dashed spectrum agrees with that of native PS I (Fig. 7 *a*, dash-dot), if the

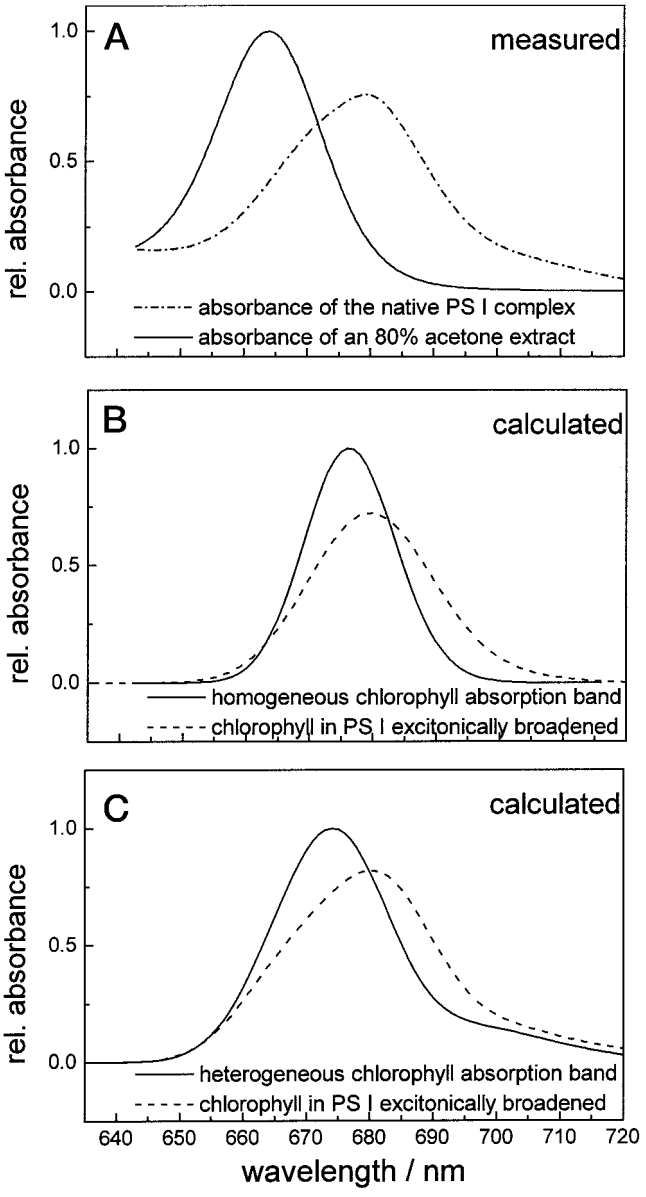

FIGURE 7 Two attempts to reproduce the absorption spectrum of the trimeric PS I complex from *S. elongatus* in the Q_Y region. (*a*) Measured absorption spectrum of trimeric PS I (*dash-dot*) and absorption spectrum of Chl *a* in 80% acetone/water (v/v). (*b*) Gaussian band representing the Q_Y absorption band of 96 spectrally identical Chls in PS I without excitonic coupling (*solid*) and with excitonic coupling (*dashed*). (*c*) Absorption of 96 Chls in PS I with heterogeneous site energies without excitonic coupling (*solid*) and with excitonic coupling (*dashed*). Taking into account spectral heterogeneity and excitonic coupling allows us to reproduce the experimental absorption spectrum of PS I (compare *dash-dotted* line in *a* and *dashed line* in *c*).

initial Gaussian band is centered at 676 nm, i.e., an additional nonspecific red shift (for discussion, see Pearlstein, 1992) of 12 nm is required to reproduce the experimentally observed red shift of 16 nm (Fig. 7 *a*). Moreover, excitonic coupling alone cannot describe the full broadening, especially the long red tail of the PS I absorption spectrum. To achieve a more satisfying simulation of the absorption in the Q_Y region, spectral heterogeneity of the Chls needs to be introduced. Fig. 7 *c* shows the absorption of 96 uncoupled Chls with identical bandwidth (FWHM = 18 nm) and heterogeneous site energies as listed in Table 2 (solid line). If all excitonic couplings are included as well (dashed line), the measured absorption spectrum of PS I shown in Fig. 7 *a* (dash dot) is reproduced closely. It should be noted that introduction of spectral heterogeneity diminishes the influence of the excitonic couplings.

As the coupling strength influences both broadening and red shifting, in the following we will discuss the limits of the point dipole approximation used for the calculation of the coupling strength. 1) Couplings calculated with the extended dipole approximation or the transition monopole approach (Chang, 1977) may differ significantly from those obtained by the point dipole approximation (see Appendix). 2) Given the shortest distances between adjacent Chls, it is presumably not sufficient to take into account only dipolar interactions (Struve, 1995). Close π-π contacts (see column 6 of Table 3), intervening chromophores (aromatic amino acid side chains, carotenoids), charge transfer interactions should be considered as well. For stacked chlorophylls in solution it was found by Kratky and Dunitz (1977) that their experimentally observed red shift considerably exceeds the one expected from excitonic calculations. 3) The dielectric constant ε of the local protein environment of the Chls is not well known.

However, calculations showed that just an unspecific increase in coupling strength did not result in satisfactory agreement with the absorption of native PS I (not shown), so that nevertheless additional heterogeneity needs to be introduced. Furthermore, spectral heterogeneity may be expected due to specific pigment-protein interactions (different coordinating ligands and hydrogen bonding with the peripheral substituents of the Chls, interaction with adjacent charged or aromatic amino acid residues, rotation of the vinyl group, nonplanarity of the Chl macrocycle).

Finally, the polarized spectra (LD and CD, see Fig. 3) give strong evidence for considerable heterogeneity among the individual Chl's site energies. Calculation of the LD based on a homogeneous absorption band (as shown in Fig. 7 *b*, dashed) and taking into account all excitonic interactions results in a large negative linear dichroism at wavelengths shorter than the absorption maximum (not shown). This is not observed in experiment (Fig. 3 *a*) and indicates the necessity for some individual Chls with positive LD to absorb at shorter wavelengths than the bulk. Regarding the CD spectrum (Fig. 3 *b*), it has been mentioned in the first section that on the blue side of the CD spectrum there is no feature corresponding to the red shoulder. This would be expected for symmetry reasons, if the transition energies of all the monomers were identical. Thus, we conclude that the absorption of the Chls associated with the red shoulder is

already red shifted without excitonic interaction. Moreover, Fig. 3 *b* shows that the zero-crossing of the CD spectra lies to the red of the isotropic absorption maximum, indicating that most of the coupled dimers are a priori red shifted with respect to the bulk, as they dominate the CD signal.

Based on the discussion above, simultaneous simulations of the optical spectra were performed using the point dipole approximation to maintain the intuitive concept of the orientation factor κ. As there is no way to assign unambiguously a color to each single chlorophyll molecule, the spectral heterogeneity was taken into account using the structural/spectral assignment as an adjustable parameter. Obviously, there may exist different assignments to reproduce the experimental results, although it turned out to be hard enough to find any that satisfies the constraints given by the set of optical spectra (see Fig. 8). Additionally, we considered the following structure-based criteria. As a general rule, we assigned equal site energies to Chls related by C_2 symmetry and coordinated by histidines, which are conserved between PsaA and PsaB. Likewise, strongly coupled Chls with similar protein-cofactor interaction were assigned the same Q_Y transition energy. The finally used structural/spectral assignment is given in Table 2 ("color" column). Fig. 8 shows simultaneously simulated absorption, LD, CD, and emission spectra in comparison with those experimentally obtained for the trimeric PS I complex from *S. elongatus*.

With the selected Chl site energies and calculated excitonic interactions, it is possible, to simulate the experimental absorption spectrum almost perfectly (Fig. 8 *a*). We conclude that both excitonic interactions and site energy disorder contribute in a comparable manner to the overall width of the experimentally observed Q_Y absorption band of PS I.

Very good agreement between simulation and experiment can also be obtained for the LD spectrum (Fig. 8 *b*). For the CD spectrum (Fig. 8 *c*), the agreement between simulation and experiment is less satisfying. This may have several reasons. CD spectra display the difference in absorption of left and right circularly polarized light. Reasons for such differences can be various, among them magnetic transitions and helical molecule structures. It is a specific property of excitonically coupled transitions, that they show two-winged conservative CD spectra. The actually observed CD signal (Fig. 8 *c*, dashed) is clearly not conservative, which was suggested to be due to mixing with higher excited (Soret-) states, the so called "hyperchromism" (Scherz and Parson, 1984). As our simulation is limited to pure Q_Y states, it cannot account for this effect and a scaling problem arises. Due to the differential nature of the CD spectrum, its bands are expected to be narrowed in comparison with the absorption bands (van Amerongen et al., 2000). In fact, the negative lobe of the experimental spectrum has a FWHM of ~16 nm, which is not reproduced by the simulation. This indicates the limits of the Gaussian dressing approach used to "flesh out" the simulated stick spectra. Obviously, in this case it would be more appropriate to use narrower homogeneous lines and to introduce additional site heterogeneity. A similar conclusion could be drawn from the red wing of the simulated emission spec-

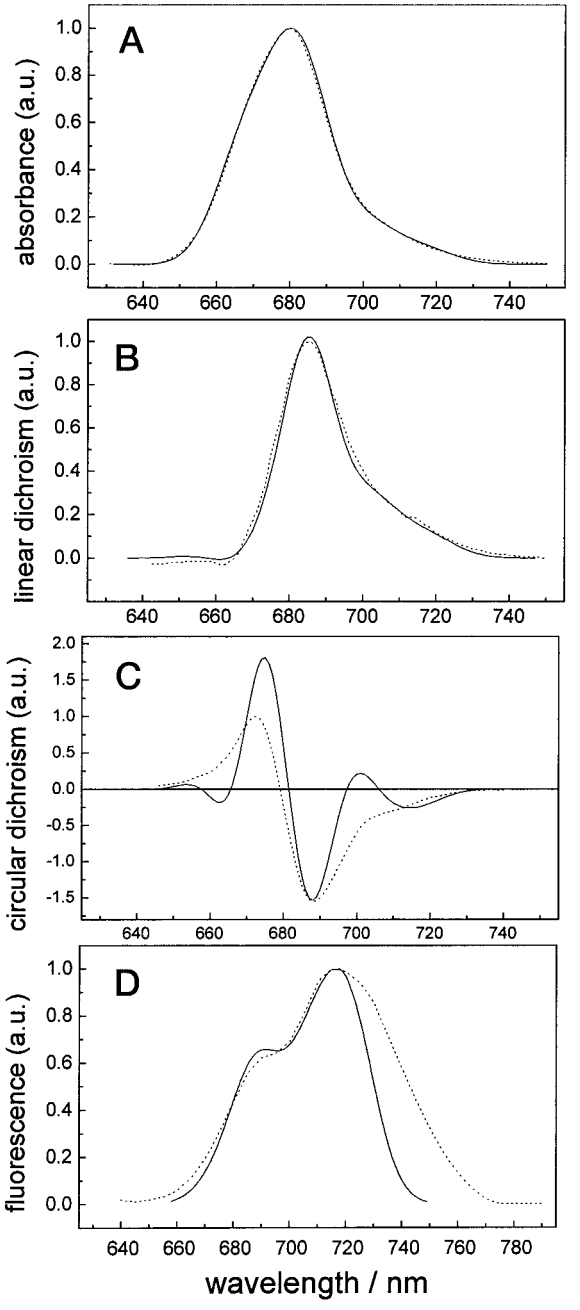

FIGURE 8 Comparison of simulated (*solid lines*) and measured (*dotted lines*) steady-state spectra (*a*) absorption, (*b*) linear dichroism, (*c*) circular dichroism, and (*d*) fluorescence emission. Whereas *a* and *b* show rather good agreement, *c* and *d* cannot reproduce the width of the experimental spectra, possibly due to the simple Gaussian dressing method used. The simulations takes into account the site energies of the Chls as in Table 2 and all excitonic interactions as calculated from the 2.5-Å structure.

trum (Fig. 8 *d*, solid) which is too narrow to meet the experimental one (Fig. 8 *d*, dashed), even after correction of the latter for the mirror image of the 630-nm band.

Localized versus Delocalized Excitation

As discussed in the previous section, excitonic interactions contribute considerably to the absorption of the PS I complex. This means that the incident light does not interact with monomeric chromophores, but instead to a considerable extend with transition moments of delocalized excitonic states. The ratio of the width (FWHM) Γ of the homogeneous absorption band and the excitonic interaction energy J determines whether the excitation should be considered as being delocalized over coupled chromophores or as being localized on uncoupled chromophores. For the excitonic interaction energy J, values of up to 250 cm^{-1} have been calculated from the structure (Table 3, even higher for P700, but see Appendix). It has been outlined before that the data for the spectral line shape of uncoupled single Chls in protein environment are sparse. The available experimental spectra are all inhomogeneously broadened, due to considerable site heterogeneity arising from both pigment-pigment and pigment-protein interactions. We determined a bandwidth of 18 nm for Chl in detergent micelles at RT and of 14 nm at 5 K (E. Schlodder, unpublished results). This is somewhat narrower than that observed for Chl in most organic solvents (Seely and Jensen, 1965) but still considerably inhomogeneously broadened. There are three recent studies of the spectroscopic properties of Chls in PS I at various temperatures (Melkozernov et al., 2000 and Rätsep et al., 2000 on *Synechocystis*; Cometta et al., 2000 on *Spirulina*). All three of them reported different widths of the absorption bands of bulk absorbing ($<$700 nm) and red absorbing ($>$700 nm) Chls. Melkozernov et al. (2000) used femtosecond absorption spectroscopy to find a homogeneous width of 120 cm^{-1} for bulk and of 240 cm^{-1} for red Chls at 77 K. Rätsep et al. (2000) burned nonphotochemical holes at 5 K and found inhomogeneous contributions of 70 cm^{-1} for bulk Chls and of 230 cm^{-1} for red Chls. Finally, Cometta et al. (2000) performed a thermal broadening analysis of a photobleaching hole and found homogeneous width of 180 cm^{-1} for bulk Chls and 350 cm^{-1} for red Chls at RT. Comparing these values with the coupling strengths as calculated reveals that none of the limiting cases $J \gg \Gamma$ or $J \ll \Gamma$ applies here. Although there are certainly interactions that are much smaller than the 100 cm^{-1} homogeneous width for bulk Chls, we argued based on the CD spectrum that tentatively the red pigments are most strongly coupled. Indeed, the strongest couplings of $>$100 cm^{-1} are comparable with the homogeneous width of the red Chls. Therefore, for the coupled aggregates from Table 3, one should keep in mind that the excitation can well be delocalized over the constituting monomers. This raises the question as to whether and to what extent the Förster mechanism is adequate for the description of the energy transfer processes as it presumes incoherent hopping of localized excitations from site to site with thermal equilibration completed on every site before further transfer occurs.

We use the delocalization parameter N_k (see Materials and Methods) as a measure for the spatial extent of an exciton state k. Taking into account all the 96 $\times$ 96 excitonic interactions between any two chlorophylls and the transition energies (colors) of the Chls as listed in Table 2, we arrive at 96 exciton states. The distribution of the N_k-values has a mean of 5.8. Only five exciton states are virtually localized ($N < 1.5$) due to Chls being rather isolated at the periphery. On the other hand, the 13 exciton states with the largest N_k-values are delocalized on average over 12 Chls; i.e., the number of Chls constituting each of these exciton states is always small compared with the total number of antenna Chls in PS I. Thus, neither the weak coupling picture with localized excitation (Förster hopping) nor the strong coupling picture with delocalized excitation (energetic relaxation between the exciton states) provide appropriate tools for the description of the energy transfer in the PS I complex. Consideration of time scales does not help either, as calculated hopping steps are quite fast, in the order of tens of femtoseconds (Table 4).

Various attempts have been undertaken to develop a unified approach incorporating both limiting cases of strong and weak coupling. Unfortunately, the most general concepts developed so far are limited to systems of only two pigments and not applicable here (Rahman et al., 1979; Struve 1995). Leegwater et al. (1997) used a "generalized Förster" approach assuming weak exciton-phonon interactions to describe excitation energy transfer within the RC of PSII. For the interaction of a single molecule with a strongly coupled aggregate, Valkunas et al. (1985) and Sumi (1999) modified the Förster overlap integral into an overlap with the density of states of the acceptor. Fetisova et al. (1996) described a modified Förster theory of excitation energy transfer between aggregates. The strong interactions between the pigments of such aggregates lead to delocalized exciton states, between which energy transfer is considered. For that, the structural factor s^2 is averaged over the Chls of each aggregate and fast thermalization between various exciton states is assumed. Thus, a Förster treatment of the excitation transfer through the PS I complex becomes possible. To maintain the picture of Förster hopping and based on the above discussed ratio of coupling strengths and bandwidth, we decided to take into account only interactions $J > 95$ cm^{-1}. If all weaker interactions are neglected, the number of the aggregates is reduced to 19 dimers and four trimers (A16/A17/A25, A31/A32/B7, B14/B15/B23, and B31/B32/B33), leaving the other 46 Chls as monomers.

TABLE 4 Simulated lifetimes for different situations with fixed parameters for intrinsic charge separation rate = 0.87 ps^{-1} and Förster radius = 78.1 Å, excitonic coupling = yes indicates that couplings >95 cm^{-1} are taken into account, decay rate of higher exciton states = 5 ps^{-1}

	Antenna Chls					
Orientation factor κ^2	Excitonic coupling	Site energy	Chls considered	Single step (fs)	Slowest transfer lifetime (ps)	Trapping lifetime (ps)
0.667	No	Homog.	All	20.6	2.4	61.6
Real	No	Homog.	All	16.8	3.3	60.0
Real	Yes	Homog.	All	61.8	3.4	25.2
Real	No	Heterog.	All	18.0	5.0	82.8
Real	Yes	Heterog.	All	70.1	4.0	34.1
Real	Yes	Heterog.	No linker clusters	68.0	4.1	34.2
Real	Yes	Heterog.	No Chls in the middle of the membrane	88.4	6.6	38.5

Shading indicates which conditions are changed between rows. For details see text.

Simulation of excitation energy transfer

Using the described simulation procedure, we now can follow quantitatively the influence of various parameters. We compared how averaged versus actual orientation factors, isolated versus coupled Chls, homogeneous versus heterogeneous site energies, and presence versus absence of certain Chls (e.g., the linker clusters) influence the transfer and trapping kinetics. The parameters for excitation and electron transfer (Förster radius R_0 and charge separation rate k_{CS}) were kept fixed throughout this section. The results are summarized in Table 4.

Averaged versus actual orientation factors

The increased resolution of the x-ray structure allows us to determine the mutual orientation of the Q_Y transition moments and, thereby, the concomitant κ^2 factors. We studied the differences arising from replacement of the previously used averaged orientation factors by the actual ones under isoenergetic conditions to separate the influence of color effects. The average orientation factor over all the 4464 pairs of Chls is found to equal 0.71 (compare Fig. 9). This value is above the average value calculated for random but fixed orientations (0.48, Maksimov and Rozman, 1961) and the average calculated under the assumption of sufficiently fast Brownian rotation of the dipoles (0.67, Förster, 1965), which has often been used erroneously. Comparison of rows 1 and 2 of Table 4 shows that a considerably faster single step hopping time with real κ^2 is accompanied by a longer transfer lifetime but only marginally faster trapping. The ratio of the hopping times (=1.23) reflects the improvement in transfer rates, which is more than just the improvement between 0.67 and 0.71 (=1.06). This demonstrates an optimization of the energy transfer between neighboring pigments. This is illustrated by Fig. 9, which shows κ^2 (circles) averaged over all pairs of Chls with center-to-center distances $R < d$, plotted versus increasing d. The number of such pairs of Chls, divided by the total number of Chls, N, is also plotted in Fig. 9 (squares). N indicates the average number of neighbors that a Chl has within a distance d.

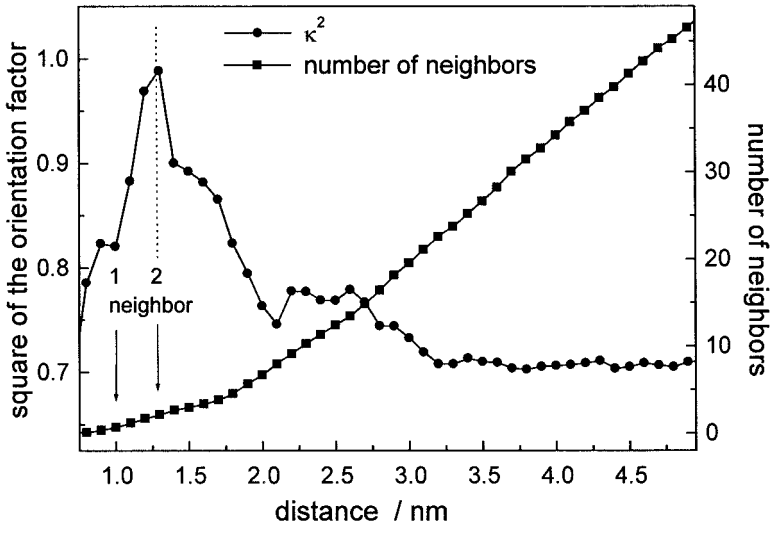

FIGURE 9 Orientation factor κ^2 (*circles*) averaged over all pairs of Chls with center-to-center distances $R < d$, plotted versus d. The number of such pairs of Chls, divided by the total number of Chls, N, is also plotted (*squares*). N indicates the average number of neighbors within a distance d. Vertical lines mark the average nearest neighbor distances for $N = 1$ and $N = 2$. Note the remarkable sharp peak in the orientation factor average exactly at the position of the two neighbor level.

Vertical lines mark the average nearest neighbor distances for $N = 1$ and $N = 2$. The average κ^2 as function of d reaches its maximal value ($\kappa^2 = 1$) at $d = 1.25$ nm, which corresponds remarkably well to $N = 2$ and then quickly falls off.

Within the stromal ring, as an example for an optimized energy transfer pathway, one finds an average κ^2 between neighboring pigments of 1.18 if exciton coupling is neglected. Taking into account the exciton coupling within the linker dimers leading to altered orientation of transition moments, this value increases to $\kappa^2 = 1.66$, i.e., more than twice the overall average. This can be taken as an indication for an optimization process towards a fast energy transfer along this ring. In the following, we will only use the actual orientation factors.

The trapping times for both averaged and actual orientation factors (Table 4, rows 1, 2) were distinctly larger than the experimental value of 34 ps. This is expected because all Chls are assumed to have the same Q_Y transition energy and the walk through the network is random, i.e., no directionality imposed. The situation changes, when spectral heterogeneity is introduced. Concomitantly, the rates for downhill energy transfer increase. Spectral heterogeneity is caused by two mechanisms: first we will consider excitonic coupling (Table 4, row 3) and second heterogeneous site energies (Table 4, row 5). For comparison, row 4 of Table 4 shows the results for a heterogeneous antenna without excitonic coupling.

Isolated versus coupled Chls in a spectrally homogeneous antenna complex

Excitonic coupling between neighboring Chls results in altered dipole strength and orientation of transition dipole moments and introduces spectral heterogeneity by energy splitting. All three effects lead to modified transfer rates. Whereas the single step hopping time and the slowest transfer lifetime increase, the trapping lifetime decreases considerably from ~60 to 25.2 ps (see row 3 of Table 4). Because the primary donor of PS I, P700 consists of the most strongly coupled pair of Chls, it absorbs at longer wavelengths than all the other pigments and the arising energy gradient towards the trap speeds up trapping.

The averaged overall effect of the altered orientation of transition dipole moments has been found to be rather small (not shown). In the following, we will discuss two especially interesting modifications of transfer rates via excitonic coupling: 1) The average κ^2 from the lumenal ring Chls to the isolated P700 Chls is ~1. Because P700 is a strongly interacting dimer, it gives rise to two new, mutually perpendicular transitions. The average κ^2 from the lumenal ring Chls to the upper exciton band of P700 is 1.1, whereas the κ^2 to the lower exciton band is 0.8. This reduces back transfer from there into the antenna, which is a competing channel to charge separation. This is especially evident for the rates from P700 to A26 and B24 that dropped below 0.3 ps^{-1} after accounting for excitonic coupling (broken lines in Fig. 6). 2) The transfer from the antenna into the lower exciton band of the linker dimers is a spectral downhill process. The transition moment of this lower band is orientated favorably towards the nearest antenna Chls. From the lower exciton band, according to Boltzmann partitioning, a considerable part of the excitation is promoted to the upper exciton band of the linker dimer. The transition moment of this band is, in turn, favorably oriented with respect to the RC and poor with respect to the antenna. As the upper band, due to the 16- to 20-nm splitting, lies above most other transitions, the excitation flow into the RC is downwards again. The Boltzmann promotion from the linker dimer's lower exciton band back into the antenna is additionally suppressed by the distribution of the oscillator strength between the two exciton bands of the linker dimers: the lower transition carries less than one-half the oscillator strength of a monomeric Chl (compare Table 3). Thus, the organization of the linker dimers enhances the directionality of the energy transfer from the antenna into the RC ("valve mechanism"). We would like to point out that the emission from the lower exciton bands of both linker dimers is supressed due to their weak oscillator strengths regardless of their considerable Boltzmann population.

Heterogeneous site energies in an excitonically coupled antenna complex

Our simulations show that the two resulting parameters (Förster radius R_0, intrinsic charge separation rate k_{CS}) as well as the calculated emission spectra (lifetimes and shapes) depend critically on the respective structural/spectral assignment of especially the red Chls. For example, the apparent trapping lifetime can be reduced both by a reduced number of red pigments and by a faster intrinsic charge separation. The transfer lifetime can be reduced both by less extended red locations and by a larger Förster radius due to larger FOI. The latter is not unequivocally known because the actual width of the Chl absorption (and emission) spectra is not accessible. If the FOI is plotted versus the difference between the transition energies of donor and acceptor, the FWHM of this curve has been reported to be ≈300 cm^{-1} by Zucchelli et al. (1998), whereas based on the spectra of Shipman et al., 1976 we obtain a width of ≈800 cm^{-1}. Thus, conclusions on the structural/spectral assignment derived from the simulation have to be used with care as long as the parameters for Förster radius and charge separation rate are not confirmed independently.

To analyze the influence of the structural/spectral assignment on the excitation energy transfer, simulations have been performed for a set of over one-thousand different assignments in the following way. The chlorophylls were assigned the wavelengths listed in column 4 of Table 2 arbitrarily with the exception of P700. The absorption of P700 has been always described by two exciton bands at

664 and 703 nm with relative oscillator strengths of 24% and 76%. Note that only the particular assignment given in Table 2 matches the measured absorption spectrum at RT (see Fig. 8 *a*).

Random structural/spectral assignments give a considerable spread in trapping lifetimes (20–200 ps), whereas the lifetime for the slowest transfer component is relatively well defined (12 ps). In 95% of the cases only one single trapping component is observed, whereas in the remaining 5% two or even more trapping components show distinctly different lifetimes. In these latter cases, red absorption was assigned to Chls, which are not connected with the reaction center by fast transfer pathways. As a consequence, the excitation energy is transiently trapped to some extent on these Chls giving rise to a faster trapping component. Uphill excitation transfer from there to the RC determines the actual trapping process and explains the slower component. In some recent experimental spectra, (Dorra et al., 1998; Gobets et al., 2001) such multiple trapping components have been resolved, which possibly could be taken as an indication for some red absorbing Chls located rather isolated at the periphery of the complex. In summary, we conclude that the excitation energy transfer dynamics is dominated by the allocation of the red absorption, whereas the detailed structural/spectral assignment of the bulk antenna Chls is of minor influence. Therefore, the next subsection will deal with the localization of the red Chls.

Where are the "red" chlorophylls localized?

In Byrdin et al. (2000) we argued in favor of localization of some red pigments in the trimerization domain. This was based on the observation of less long-wavelength absorption in monomeric PS I complexes. Similar results are reported by Rätsep et al. (2000) for *Synechocystis*. Based on the 2.5-Å structure of *S. elongatus*, we propose the tightly coupled cluster A31-A32-B7-B6 close to the trimerization domain (Fig. 4 *a*, top) for this role. The strongest excitonic splitting (~20 nm) occurs between two pigments (A32 and B7) that are bound by different subunits and in contact to a third (the PsaL) subunit. Obviously, this location is very sensitive both to the lack of the PsaL subunit in a deletion mutant and to the loss of PsaL by detergent treatment. Additionally, B7 is unique for this side of the complex and has no C_2-symmetry analogue on the opposite side.

Some other red absorbing pigments were suggested (Byrdin et al., 2000 and references therein) to be located near the linker positions so as to facilitate concentration of excitation in the vicinity of P700. The 2.5-Å structure here readily suggests the linker dimers A38/39 and B37/38 as candidates. Both are strongly coupled (~20 nm splitting for B37/38 and ~16 nm splitting for A38/39, Table 3). Other strongly coupled aggregates such as the trimer B31-B32-B33 close to PsaX (Jordan et al., 2001) and/or the dimer A12-A14 close to PsaK with an excitonic splitting >20 nm may or may not contribute to the long-wavelength absorption, depending on the transition energy of the participating monomers. The suggested candidates of red Chls are sufficiently well integrated in the network (compare Fig. 6). Given an appropriate spectral assignment of neighbouring Chls, which facilitate excitation transfer to the RC, they do not form pseudo-traps that have been found to be responsible for a second trapping component.

Based on these considerations, various sets of structural/spectral assignment of the red Chls have been tested by simulations. The structural/spectral assignment listed in the "color" column of Table 2 turned out to be most satisfying for the simultaneous simulation of both the steady-state optical spectra (Fig. 8) and the excitation energy transfer dynamics (Table 4, row 5). The trapping lifetime calculated based on this special structural/spectral assignment agrees well with the experimentally observed fluorescence lifetimes of ~34 ps (see Introduction). Recent experiments (Dorra et al., 1998; Savikhin et al., 1999; Byrdin et al., 2000; Gobets et al., 2001, Kennis et al., 2001) still show a considerable spread in the lifetimes and spectra of the transfer components. However, two most recent studies with the highest time resolution agree well with the lifetime of the slowest transfer component (~4 ps) of our simulation. The spectral shape of this transfer component was found to be strongly excitation wavelength dependent (Hastings et al., 1995). Our simulations confirm the inversion of the transfer spectrum upon change from blue to red excitation (not shown).

Interestingly, the single step hopping time in the energetically heterogeneous situation (70.1 fs, Table 4, row 5) is slower compared with the homogeneous situation (16.8 fs, Table 4, row 2), but is similar to the situation where heterogeneity was introduced solely via excitonic coupling (61.8 fs, Table 4, row 3). This indicates that excitonic coupling decreases spectral overlap between spatially adjacent Chls in comparison with the homogeneous (isoenergetic) situation resulting in a rather rugged energy landscape.

Using the described structural/spectral assignment, we analyzed the role of the linker clusters for efficient excitation energy trapping. Removing the linker clusters in our simulation had nearly no effect on the trapping time (Table 4, row 5 and 6). If all antenna Chls located in the middle of the membrane (see Table 2) are omitted in the simulation, the trapping time increases slightly from 34.1 to 38.5 ps (see Table 4, row 7). If the color of all long-wavelength transitions ("red" Chls) was changed to 680 nm in the simulation, the trapping time decreased to 20.1 ps in accordance with experimentally observed trapping times in PS I complexes with a low content of "red" Chls (see e.g., Gobets et al., 2001). The rather small changes of the trapping time are taken as further evidence for the remarkable robustness of the overall excitation energy transfer in PS I. In summary,

the spread between longest and shortest trapping lifetimes found for different situations (see Table 4) is approximately threefold. Note that this corresponds to a difference in quantum efficiency of only 3% between ~98% and ~95%.

Parameters for excitation transfer and primary charge separation

The intrinsic rate of primary charge separation for the PS I complex cannot be directly measured because of the preceding excitation energy transfer. Both processes together determine the measured transfer and trapping times. Earlier calculations were limited to equilibrium considerations and had to assume that the distribution of excitation over the different spectral forms can be calculated according to Boltzmann. But charge separation is not necessarily sufficiently slow to allow thermal equilibration of the excitations within the PS I complex. Our simulations are not hampered by such limitation and can provide insight into the degree of thermal equilibration. In fact, the presence of charge separation leads to a nonequilibrated steady state. In Fig. 10 *a*, the spectral shape of the resulting emission (solid) is compared with that resulting from a system without charge separation, i.e., emission from a thermally equilibrated system (dashed). The spectra are normalized to equal area. Fig. 10 *a* shows that there is less red emission with charge separation than without it. This means that the trapping of the excitation energy proceeds mainly from the red Chls, which leads to their reduced population with respect to thermal equilibrium.

In the following we ask for the rate limiting step of efficient light harvesting in PS I. Two processes are discussed for this role: excitation energy transfer, governed by the Förster radius R_0 and trapping, governed by the intrinsic charge separation rate k_{CS}. A twofold increase or decrease of the transfer speed with fixed k_{CS} results in 28- and 45-ps trapping lifetimes instead of the originally 34 ps. Corresponding variations of k_{CS} with fixed R_0 renders lifetimes of 23 and 56 ps. Both influences on the trapping rate are comparable, although that of k_{CS} is slightly stronger. This suggests that the excited state dynamics is neither pure trap limited, nor pure transfer (to the trap) limited, but seems to be rather balanced. Major variations in the parameters resulted in minor effects on the trapping lifetime indicating, on one hand, the robustness of the system with respect to distortions. On the other hand, it complicates the evaluation of the correct parameters. The observed fluorescence lifetime of 34 ps can be achieved in the simulations by numerous combinations of parameters. Fig. 10 *b* shows the charge separation rate required for a 34-ps trapping time as a function of Förster radius using the spectral/structural assignment given in Table 2. For slow transfer (left hand side), very fast charge separation is necessary (>2 ps^{-1}), but even for (almost) infinitely fast transfer (right hand side), i.e., for the trap limited case, the charge separation rate has to be as fast as 0.7 ps^{-1}. The actual transfer speed is defined by the lifetime of the slowest experimentally resolved transfer spectrum (~4 ps, Gobets et al., 2001; Kennis et al., 2001) which corresponds to an isoenergetic Förster radius of 7.8 nm (indicated by an arrow in Fig. 10 *b*). The resulting rate of primary charge separation equals 0.87 ps^{-1} (~1.1 ps), which makes the PS I core complex the system with the fastest known primary charge separation rate.

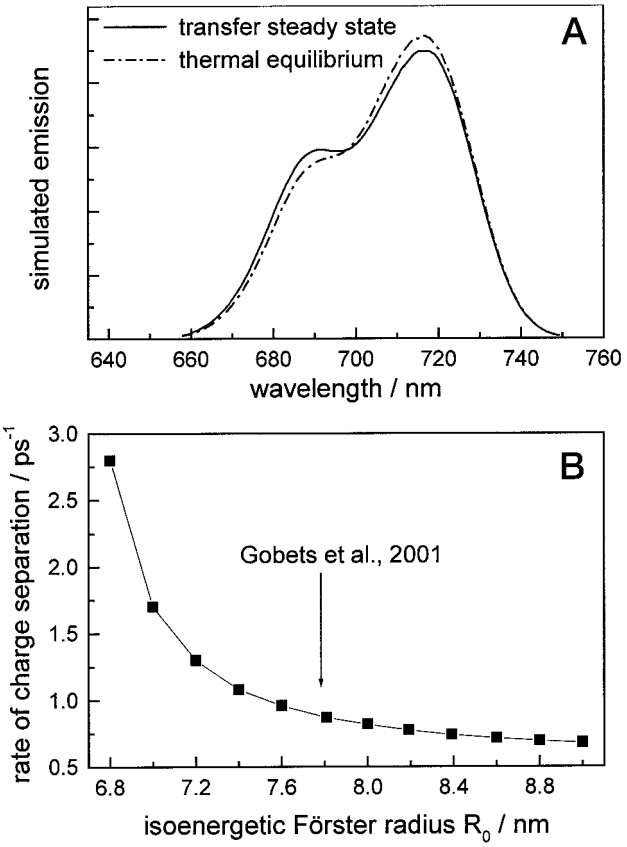

FIGURE 10 (*a*) Simulated fluorescence emission of the PS I core complex from *S. elongatus* with (*solid*) and without (*dashed*) charge separation. Curves are normalized to equal area. Note that charge separation introduces a deficit in red emission. (*b*) Plot of intrinsic charge separation rate required at a given transfer speed (abscissa) to obtain a trapping lifetime of 34 ps. The arrow indicates a Förster radius of 7.8 nm corresponding to a charge separation rate of 0.87 ps^{-1}. For details see text.

CONCLUSIONS

In this work, we used exciton coupling theory to simultaneously model absorption, excitation transfer and emission spectra of the PS I complex from *S. elongatus* based on the 2.5-Å x-ray structure (Jordan et al., 2001).

Excitonic coupling contributes considerably to both the broadening and red shift of the Q_Y absorption band of PS I as compared with that of Chl in organic solvents. In addition, site energy disorder due to pigment-protein interac-

tions is required to reproduce the inhomogeneously broadened Q_Y absorption band of PS I.

Most of the chlorophylls are located within two layers, one close to the stromal, the other close to the lumenal membrane surface. A ring-shaped arrangement of pigments within each of these layers surrounds the RC of PS I. Energy transfer between neighboring Chls forming the rings is sufficiently fast to assure efficient flow of excitation energy through the antenna system. The Chls of these two rings are well connected among each other via Chls located within the membrane and with chlorophylls located peripherally on the stromal and lumenal side, respectively.

Such an arrangement facilitates fast distribution of the excitation energy over the whole antenna complex and is able to rationalize the observed short transfer times. Monte Carlo simulations revealed that the excitation energy transfer to the trap (RC) occurs to a large extent via the linker clusters, although the larger part is contributed by all the other Chls. The linker clusters are suggested to have a red shifted absorption due to both strong coupling and low site energy. Their organization enhances the directionality of the energy transfer from the antenna into the RC.

Excitation transfer simulations showed that the modeled trapping lifetime depends on all three parameters invoked: rate of intrinsic charge separation and rate of isoenergetic Förster transfer (Förster radius), and, most critical, on the spectral/structural assignment. The parameters derived from the modeling suggest both fast transfer (Förster radius 7.8 nm) and fast trapping (intrinsic primary charge separation rate 0.87 ps^{-1}). Variation of all three parameters reveals that the excited state dynamics is neither pure trap limited, nor pure transfer (to the trap) limited, but seems to be well balanced and that the system is optimized rather for robustness than for extremely fast trapping.

APPENDIX

Extended dipole approximation describes well the spectral features of the RC

In the extended dipole approximation, one sums over the pairwise Coulomb interaction of four point monopoles instead of two point dipoles (Pearlstein, 1992). For energies in cm^{-1}, each term of the sum can be expressed in the form $\pm 5.04\ \mu^2/(r_{is,jt}D^2)$, in which $r_{is,jt}$ is the distance in nanometers from the sth charge on the ith molecule to the tth charge on the

TABLE A1 Excitonic interaction between the Chls within the reaction center

***(a)* Pairwise excitonic interaction energies (cm^{-1}), calculated by the point dipole approximation (upper right) and the extended dipole approximation (lower left)**

Point dipole extended dipole	S1	S2	S3	S4	S5	S6
S1 (P700.A)		414.8	−92.1	−25.1	14.4	6.6
S2 (P700.B)	138.3		−24.1	−87.0	5.9	13.5
S3 (Acc.B)	−104.8	−26.2		28.2	157.4	−9.3
S4 (Acc.A)	−27.3	−98.8	31.0		−10.3	189.4
S5 (Ao.A)	14.0	5.6	130.5	−10.4		2.7
S6 (Ao.B)	6.4	12.9	−9.4	141.6	2.6	

***(b)* Eigenvalues in nm, oscillator strengths and eigenvectors resulting from calculations within the point dipole and extended dipole [ ] approximation**

Wavelength/nm (rel. Osc.-strength) for point dipole all Chls initially at 680 nm [for extended dipole all Chls initially at 690 nm]	S1 (P700.A)	S2 (P700.B)	S3 (Acc.B)	S4 (Acc.A)	S5 (Ao.A)	S6 (Ao.B)
660 (0.40)	+0.68	+0.68	−0.2	−0.2	−0.03	−0.05
[679 (0.36)]	[+0.52]	[+0.52]	[−0.43]	[−0.44]	[−0.18]	[−0.21]
672 (0.72)	−0.14	−0.06	+0.11	−0.67	+0.11	−0.71
[683 (1.06)]	[−0.16]	[+0.07]	[+0.47]	[−0.50]	[+0.46]	[−0.54]
673 (0.46)	+0.10	+0.16	+0.67	0.08	+0.71	+0.09
[686 (0.10)]	[+0.39]	[+0.42]	[+0.30]	[+0.22]	[+0.56]	[+0.47]
687 (1.27)	−0.04	−0.17	−0.66	−0.22	+0.66	+0.23
[694 (0.20)]	[−0.49]	[+0.55]	[+0.31]	[−0.23]	[−0.43]	[+0.34]
689 (1.07)	+0.19	−0.09	−0.22	+0.66	+0.21	−0.65
[697 (1.37)]	[−0.31]	[−0.19]	[−0.47]	[−0.51]	[+0.41]	[+0.47]
700 (2.08)	−0.69	+0.69	−0.15	+0.14	+0.07	−0.08
[700 (2.91)]	[+0.46]	[−0.46]	[+0.43]	[−0.45]	[−0.30]	[+0.33]

*j*th molecule, μ^2 is the strength of the transition in Debye^2, $D = 0.6$ nm is the extend of the charge distribution on the Chl molecule, and the sign $+(-)$ is for like (unlike) charges.

For distances comparable with or smaller than the extent of the charge distribution, the point dipole approximation must be used with care. For calculation of the spectral properties of the six coupled Chls within the RC it is reasonable to work with the extended dipole approximation. Whereas all other coupling strengths change only slightly if the extended dipole approximation is used instead of the point dipole approximation, the interaction energy within P700 decreases threefold. This has several consequences. 1) It allows to work with increased coupling strengths, as it takes away the limitation introduced by the upper exciton band of P700. 2) The number of pigments with stronger coupling than in P700 increases from none to more than 20. 3) Whereas it is almost impossible to simultaneously simulate the P/P^+ difference absorption (E. Schlodder, unpublished) and P/P^+ difference CD (Karapetyan et al., 1984) spectra with the couplings resulting from the point dipole approximation, this is easily accomplished with the extended dipole coupling values (Table A1, simulations not shown).

Along with the decreased coupling between the two P700 Chls, the couplings to their respective neighbors (the accessories) are increased so that all of the coupling energies between neighboring Chls in the RC become comparable. The couplings between the Chls within the RC have also been calculated using the more accurate point monopole method (Chang, 1977), which has been more recently applied to structure-based calculations of the optical spectra of the LH2 complex from *Rps. acidophila* (Sauer et al., 1996). Interestingly, this approach agrees with the extended dipole approximation on the result that all of the coupling energies between neighboring Chls in the RC are of comparable strength. As a consequence, the RC of PS I has to be considered as a "superaggregate" instead of three dimers. Furthermore, the excited singlet states in the reaction center, corresponding to exciton states, are most probably delocalized over the six Chls. Concomitantly, the "P700" band consists of two closely spaced bands at 697 and 700 nm, both of which have almost equal contributions from all six RC Chls, carrying together the oscillator strength of four isolated transitions. This could explain the failure of attempts to identify the "upper P band" (Brettel, 1997). The oscillator strength of one Chl is found at 683 nm, a region where features in the difference spectra were assigned to A_0, which also does not appear in this picture as a separate species. Finally, we would like to point out that this latter feature at 683 nm correlates well with the resonant photo-bleaching band observed by Melkozernov et al. (2000) upon excitation at 700 nm. Thus, the extended dipole approximation appears to be a promising approach for further understanding of the spectral changes related to the primary processes in the PS I reaction center.

We thank Dr. Margitta Dathe and Heike Nikolenko from the Institute of Molecular Pharmacology Berlin for kind support with the CD recording, Marianne Çetin for excellent technical assistance, and Heike Witt for critical reading of the manuscript. M. B. wants to thank H.-W. Trissl and K. Brettel for helpful discussions.

This research was supported by the Deutsche Forschungsgemeinschaft (Sonderforschungsbereich 498, TP A1, A3, A4).

REFERENCES

Arnett, D. C., C. C. Moser, P. L. Dutton, and N. F. Scherer. 1999. The first events in photosynthesis: electronic coupling and energy transfer dynamics in the photosynthetic reaction center from rhodobacter sphaeroides. *J. Phys. Chem. B.* 103:2014–2032.

Beekman, L. M. P., R. N. Frese, G. J. S. Fowler, R. Picorel, R. J. Cogdell, I. H. M. van Stokkum, C. N. Hunter, and R. van Grondelle. 1997. Characterization of the light harvesting antennas of photosynthetic purple bacteria by stark spectroscopy: 2. LH2 complexes: influence of the protein environment. *J. Phys. Chem. B.* 101:7293–7301.

Brettel, K. 1997. Electron transfer and arrangement of the redox cofactors in photosystem I. *Biochim. Biophys. Acta.* 1318:322–373.

Byrdin, M., I. Rimke, E. Schlodder, D. Stehlik, and T. A. Roelofs. 2000. Decay kinetics and quantum yields of fluorescence in photosystem I from *Synechococcus elongatus* with P700 in the reduced and oxidized state: are the kinetics of excited state decay trap-limited or transfer-limited? *Biophys. J.* 79:992–1007.

Chang, J. C. 1977. Monopole effects on electronic excitation interactions between large molecules: I. Application to energy transfer in chlorophylls. *J. Chem. Phys.* 67:3901–3909.

Colbow, K. 1973. Energy transfer in photosynthesis. *Biochim. Biophys. Acta.* 314:320–327.

Cometta, A., G. Zucchelli, N. V. Karapetyan, E. Engelmann, F. M. Garlaschi, and R. C. Jennings. 2000. Thermal behavior of long wavelength absorption transitions in *Spirulina platensis* Photosystem I trimers. *Biophys. J.* 79:3235–3243.

Deisenhofer, J., O. Epp, K. Miki, R. Huber, and H. Michel. 1985. Structure of the protein subunits in the photosynthetic reaction center of *Rhodopseudomonas viridis* at 3 Å resolution. *Nature.* 318:618.

Dexter, D. L. 1953. A theory of sensitized fluorescence in solids. *J. Chem. Phys.* 21:836–850.

Dorra, D., P. Fromme, N. V. Karapetyan, and A. R. Holzwarth. 1998. Fluorescence kinetics of photosystem I: multiple fluorescence components. *In* Proceedings of the XIth International Photosynthesis Congress. G. Garab, editor. Kluwer Academic Publishers, Dordrecht. 587–590.

Du, M., X. Xie, Y. Jia, L. Mets, and G. R. Fleming. 1993. Direct observation of ultrafast energy transfer in PS I core antenna. *Chem. Phys. Lett.* 201:535–542.

Durrant, J. R., D. R. Klug, S. L. S. Kwa, R. van Grondelle, G. Porter, and J. P. Dekker. 1995. A multimer model for P680, the primary electron donor of photosystem II. *Proc. Natl. Acad. Sci. U.S.A.* 92:4798–4802.

Engelmann, E., T. Tagliabue, N. V. Karapetyan, F. M. Garlaschi, G. Zucchelli, and R. C. Jennings. 2001. CD spectroscopy provides evidence for excitonic interactions involving red-shifted chlorophyll forms in photosystem I. *FEBS Letts.* 499:112–115.

Fenna, R. E., and B. W. Matthews. 1975. Chlorophyll arrangement in a bacteriochlorophyll protein from *Chlorobium limicola*. *Nature.* 258:573.

Fetisova, Z., A. Freiberg, K. Mauring, V. Novoderezhkin, A. Taisova, and K. Timpmann. 1996. Excitation energy transfer in chlorosomes of green bacteria: theoretical and experimental studies. *Biophys. J.* 71:995–1010.

Fidder, H., J. Knoester, and D. A. Wiersma. 1991. Optical properties of disordered molecular aggregates: a numerical study. *J. Chem. Phys.* 95:7880–7890.

Förster, Th. 1965. Delocalized excitation and excitation transfer. *In* Modern Quantum Chemistry. O. Sinanoğlu, editor. Academic Press, New York. IIIB:93–137.

Fromme, P., and H. T. Witt. 1998. Improved isolation and crystallization of photosystem I for structural analysis. *Biochim. Biophys. Acta.* 1365: 175–184.

Gobets, B., H. van Amerongen, R. Monshouwer, J. Kruip, M. Rögner, R. van Grondelle, and J. P. Dekker. 1994. Polarized site-selected fluorescence spectroscopy of isolated photosystem I particles. *Biochim. Biophys. Acta.* 1188:75–85.

Gobets, B., I. H. M. van Stokkum, M. Rögner, J. Kruip, E. Schlodder, N. Karapetyan, J. P. Dekker, and R. van Grondelle. 2001. Time resolved fluorescence emission measurements of photosystem I particles of various cyanobacteria: a unified compartmental model. *Biophys. J.* 81: 407–424.

Golbeck, J. H. 1994. Photosystem I in cyanobacteria. *In* The Molecular Biology of Cyanobacteria. D. A. Bryant, editor. Kluwer Academic Publishers, Dordrecht. 319–360.

Gradinaru, C. C., S. Özdemir, D. Gülen, I. H. M. van Stokkum, R. van Grondelle, and H. van Amerongen. 1998. The flow of excitation energy in LHCII monomers: implications for the structural model of the major plant antenna. *Biophys. J.* 75:3064–3077.

Hastings, G., L. J. Reed, S. Lin, and R. E. Blankenship. 1995. Excited state dynamics in photosystem I: effects of detergent and excitation wavelengths. *Biophys. J.* 69:2044–2055.

Holzwarth, A. R., G. Schatz, H. Brock, and E. Bittersmann. 1993. Energy transfer and charge separation kinetics in photosystem I. Part I: picosecond transient absorption and fluorescence study of cyanobacterial photosystem I particles. *Biophys. J.* 64:1813–1826.

Jelezko, F., C. Tietz, U. Gerken, J. Wrachtrup, and R. Bittl. 2000. Single-molecule spectroscopy on photosystem I pigment-protein complexes. *J. Phys. Chem. B.* 104:8093–8096.

Jordan, P., P. Fromme, H. T. Witt, O. Klukas, W. Saenger, and N. Krauß. 2001. Three-dimensional structure of cyanobacterial photosystem I at 2.5 Å resolution. *Nature.* 411:909–917.

Karapetyan, N. V., D. Dorra, G. Schweitzer, I. N. Bezsmertnaya, and A. R. Holzwarth. 1997. Fluorescence spectroscopy of the longwave chlorophylls in trimeric and monomeric photosystem I core complexes from the cyanobacterium *Spirulina platensis*. *Biochemistry.* 36:13830–13837.

Karapetyan, N. V., V. V. Shubin, M. G. Rakhimberdieva, R. G. Vashchenko, and Yu. V. Bolychevtseva. 1984. Structural organization of photosystem I reaction centers. *FEBS Letts.* 173:209–212.

Kennis, J. T. M., B. Gobets, I. H. M. van Stokkum, J. P. Dekker, R. van Grondelle, G. R. Fleming. 2001. Light harvesting by chlorophylls and carotenoids in the photosystem I core complex of *Synechococcus elongatus*: a fluorescence upconversion study. *J. Phys. Chem.* 105: 4485–4494.

Klug, D. R., J. R. Durrant, and J. Barber. 1998. The entanglement of excitation energy transfer and electron transfer in the reaction center of photosystem II. *Phil. Trans. R. Soc. Lond. A.* 356:449–464.

Knapp, E. W., S. F. Fischer, W. Zinth, M. Sander, W. Kaiser, J. Deisenhofer, and H. Michel. 1985. Analysis of optical spectra from single crystals of *Rhodopseudomonas viridis* reaction centers. *Proc. Natl. Acad. Sci. U.S.A.* 82:8463–8467.

Koepke, J., X. Hu, C. Münke, K. Schulten, and H. Michel. 1996. The crystal structure of the light harvesting complex II (B800–850) from *Rhodospirillum molischianum*. *Structure.* 4:581–597.

Kratky, C., and J. D. Dunitz. 1977. Ordered aggregation states of chlorophyll a and some derivatives. *J. Mol. Biol.* 113:431–442.

Krueger, B. P., G. D. Scholes, and G. R. Fleming. 1998. Calculation of couplings and energy-transfer pathways between the pigments of LH2 by the ab initio transition density cube method. *J. Phys. Chem.* 102: 5378–5386.

Kühlbrandt, W., D. N. Wang, and Y. Fujiyoshi. 1994. Atomic model of plant light-harvesting complex by electron crystallography. *Nature.* 367: 614–621.

Laible, P. D. 1995. The first 100 picoseconds of photosynthesis: excited state energy transfer and trapping in photosystem I. PhD Thesis, Cornell University.

Laible, P. D., R. S. Knox, and T. G. Owens. 1998. Detailed balance in Förster-Dexter excitation transfer and its application to photosynthesis. *J. Phys. Chem. B.* 102:1641–1648.

Leegwater, J. A., J. R. Durrant, and D. R. Klug. 1997. Exciton equilibration induced by phonons: theory and applications to PS II reaction centers. *J. Phys. Chem. B,* 101:7205–7210.

Maksimov, M. Z., and I. M. Rozman. 1961. On energy transfer in solid solutions. *Opt. Spectr.* (*USSR*). [English Translation] 12:337–338.

McDermott, G., S. M. Prince, A. A. Freer, A. M. Hawthornthwaite-Lawless, M. Z. Papiz, R. J. Cogdell, and N. W. Isaacs. 1995. Crystal structure of an integral membrane light-harvesting complex from photosynthetic bacteria. *Nature.* 374:517–521.

Melkozernov, A. N., S. Lin, and R. E. Blankenship. 2000. Femtosecond transient spectroscopy and excitonic interactions in photosystem I. *J. Phys. Chem. B.* 104:1651–1656.

Owen, G. M., and A. J. Hoff. 2001. Absorbance detected magnetic resonance spectra of the FMO complex of *Prosthecochloris aestuarii* reconsidered: exciton simulations. *J. Phys. Chem. B.* 105:1458–1463.

Pålsson, L.-O., C. Flemming, B. Gobets, R. van Grondelle, J. P. Dekker, and E. Schlodder. 1998. Energy transfer and charge separation in photosystem I: P700 oxidation upon selective excitation of the long-wavelength antenna chlorophylls of *Synechococcus elongatus*. *Biophys. J.* 74:2611–2622.

Pearlstein, R. M. 1992. Theoretical interpretation of antenna spectra. *In* Chlorophylls. H. Scheer, editor. CRC Press, Boca Raton, FL. 1047–1078.

Rahman, T. S., R. S. Knox, and V. M. Kenkre. 1979. Theory of depolarization of fluorescence in molecular pairs. *Chem. Phys.* 44:197–211.

Rätsep, M., T. W. Johnson, P. R. Chitnis, and G. J. Small. 2000. The red-absorbing chlorophyll a antenna states of photosystem I: a hole-burning study of *Synechocystis* sp. PCC 6803 and its mutants. *J. Phys. Chem. B.* 104:836–847.

Sauer, K., R. J. Cogdell, S. M. Prince, A. Freer, N. W. Isaacs, and H. Scheer. 1996. Structure-based calculations of the optical spectra of the LH2 bacteriochlorophyll-protein complex of *Rhodopseudomonas acidophila*. *Photochem. Photobiol.* 64:564–576.

Savikhin, S., W. Xu, P. R. Chitnis, and W. S. Struve. 2000. Ultrafast primary processes in photosystem I of *Synechocystis* PCC 6803: roles of P700 and A_0. *Biophys. J.* 79:1573–1586.

Savikhin, S., W. Xu, V. Soukoulis, P. R. Chitnis, and W. S. Struve. 1999. Ultrafast primary processes in photosystem I of *Synechocystis* sp. PCC 6803. *Biophys. J.* 76:3278–3288.

Scherz, A., and W. W. Parson. 1984. Exciton interactions in dimers of bacteriochlorophyll and related molecules. *Biochim. Biophys. Acta.* 766: 666–678.

Schubert, W.-D., O. Klukas, N. Krauß, W. Saenger, P. Fromme, and H. T. Witt. 1997. Photosystem I of *Synechococcus elongatus* at 4 Å resolution: comprehensive structure analysis. *J. Mol. Biol.* 272:741–769.

Schulten, K. 1999. From simplicity to complexity and back: function, architecture, and mechanism of light-harvesting systems in photosynthetic bacteria. *In* Simplicity and Complexity in Proteins and Nucleic Acids. H. Frauenfelder, J. Deisenhofer, and P. G. Wolynes, editors. Dahlem University Press, Berlin. 227–253.

Seely, G. R., and R. G. Jensen. 1965. Effect of solvent on the spectrum of chlorophyll. *Spectrochim. Acta.* 21:1835–1845.

Shipman, L. L. 1977. Oscillator and dipole strength for chlorophyll and related molecules. *Photochem. Photobiol.* 26:287–292.

Shipman, L. L., T. M. Cotton, J. R. Norris, and J. J. Katz. 1976. An analysis of the visible absorption spectrum of chlorophyll *a* monomer, dimer, and oligomers in solution. *J. Am. Chem. Soc.* 98:8222–8230.

Soukoulis, V., S. Savikhin, W. Xu, P. R. Chitnis, and W. S. Struve. 1999. Electronic spectra of photosystem I mutants: the peripheral subunits do not bind red chlorophylls in *Synechocystis* PCC 6803. *Biophys. J.* 76:2711–2715.

Struve, W. S. 1995. Theory of electronic energy transfer. *In* Anoxygenic Photosynthetic Bacteria. R. E. Blankenship, M. T. Madigan, and C. E. Bauer, editors. Kluwer Academic Publishers, Dordrecht 297–313.

Sumi, H. 1999. Theory on rates of excitation energy transfer between molecular aggregates through distributed transition dipoles with application to the antenna system in bacterial photosynthesis. *J. Phys. Chem. B.* 103:252–260.

Sundström, V., T. Pullerits, and R. van Grondelle. 1999. Photosynthetic light harvesting: reconciling dynamics and structure of purple bacterial LH2 reveals function of photosynthetic unit. *J. Phys. Chem. B.* 103: 2327–2346.

Trinkunas, G., and A. R. Holzwarth. 1996. Kinetic modeling of exciton migration in photosynthetic systems: 3. Application of genetic algorithms to simulations of excitation dynamics in three-dimensional photosystem I core-antenna-RC-complexes. *Biophys. J.* 71:351–364.

Trissl, H.-W. 1993. Long wavelength absorbing antenna pigments and heterogeneous absorption bands concentrate excitons and increase absorption cross section. *Photosynth. Res.* 35:247–263.

Valkunas, L., S. Kudzmauskas, and G. Juzliunas. 1985. The process of electron excitation transfer in a highly concentrated solution of pseudoisocyanine dye. *Litovskii Fizicheskii Sbornik.* 26:54–60.

Van Grondelle, R., J. P. Dekker, T. Gillbro, and V. Sundström. 1994. Energy transfer and trapping in photosynthesis. *Biochim. Biophys. Acta.* 1187:1–65.

van Amerongen, H., L. Valkunas, and R. van Grondelle. *Photosynthetic Excitons.* 2000. World Scientific, Singapore.

van der Lee, J., D. Bald, S. L. S. Kwa, R. van Grondelle, M. Rögner, and J. P. Dekker. 1993. Steady-state polarized light spectroscopy of isolated Photosystem I complexes. *Photosynth. Res.* 35:311–321.

Vos, M. H., J. Breton, and J.-L. Martin. 1997. Electronic energy transfer within the hexamer cofactor system of bacterial reaction centers. *J. Phys. Chem. B.* 101:9820–9832.

Zouni, A., H.-T. Witt, J. Kern, P. Fromme, N. Krauß, W. Saenger, and P. Orth. 2001. Crystal structure of photosystem II from *Synechococcus elongatus* at 3.8 Å resolution. *Nature.* 409:739–743.

Zucchelli, G., O. Cremonesi, F. M. Garlaschi, and R. C. Jennings. 1998. Förster overlap integral for chlorophyll a in a protein matrix. *In* Proceedings of the XIth International Photosynthesis Congress. G. Garab, editor. Kluwer Academic Publishers, Dordrecht. 449–452.